

## *Supporting Informations for Theranostics*

### Esterase-responsive albumin-binding PROTAC-mediated BRD4 degradation for cancer immunotherapy

Hoyeon Lee<sup>1,2,#</sup>, Sojin Jeong<sup>1,#</sup>, Juwon Park<sup>1,#</sup>, Hye-jeong Son<sup>3</sup>, Seho Kweon<sup>3</sup>, Steve Seung-Young Lee<sup>4</sup>, Nayeon Shim<sup>1</sup>, Yoojeong Oh<sup>1</sup>, Hyein Kang<sup>1,2</sup>, Chaerin Lee<sup>1,2</sup>, Jihyeon Lee<sup>1,2</sup>, Jinseong Kim<sup>1</sup>, Hanhee Cho<sup>1,5,\*</sup>, Kwangmeyung Kim<sup>1,2,\*</sup>

<sup>1</sup>College of Pharmacy, Graduate School of Pharmaceutical Sciences, Ewha Womans University, Seoul, 03760, Republic of Korea.

<sup>2</sup>Graduate Program in Innovative Biomaterials Convergence, Ewha Womans University, Seoul 03760, Korea.

<sup>3</sup>College of Pharmacy, Chonnam National University, Gwangju 61186, Republic of Korea.

<sup>4</sup>Department of Pharmaceutical Sciences, University of Illinois Chicago, Chicago, IL, USA

<sup>5</sup>Noxpharm Co., LTD., Seoul 03759, Republic of Korea

<sup>#</sup>These authors contributed equally to this work.

\*Correspondence and requests for materials should be addressed to **H. Cho** (E-mail: hanheecho31@gmail.com) and **K. Kim** (E-mail: [kimkm@ewha.ac.kr](mailto:kimkm@ewha.ac.kr))

## Supporting Figures

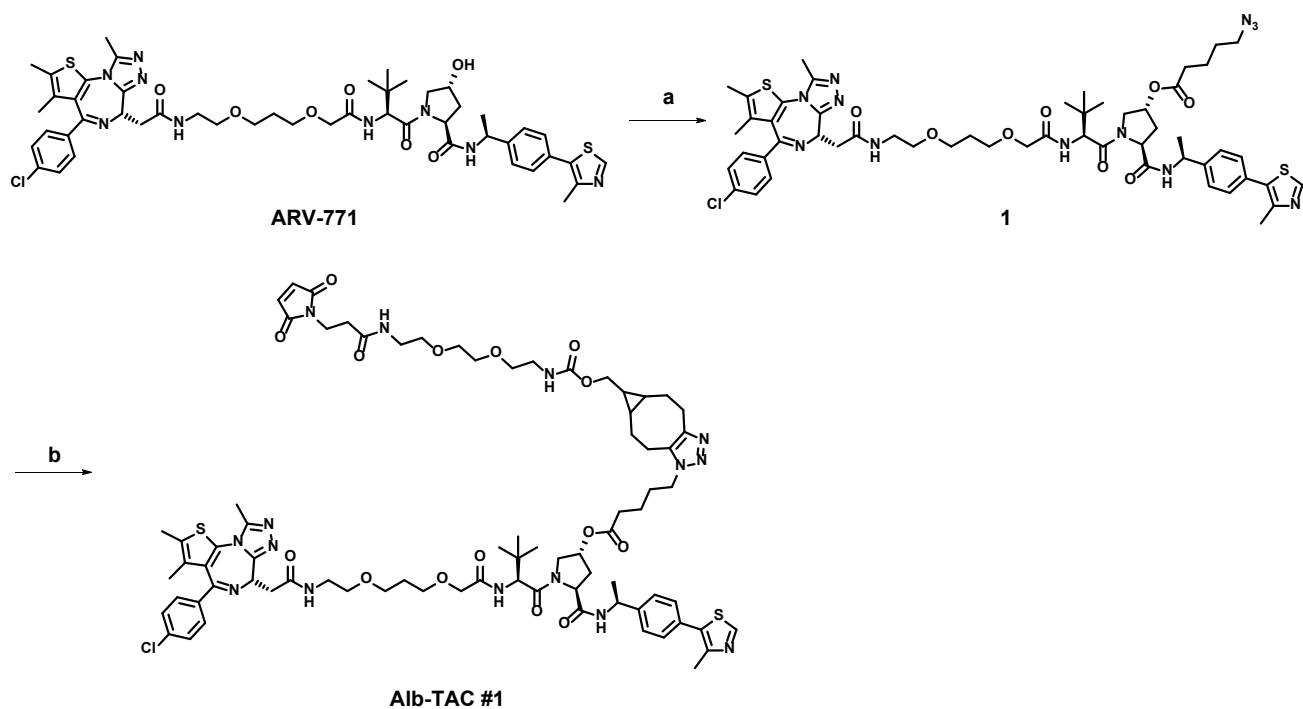


**Figure S1. Synthetic scheme of Alb-TAC #1.** Schematic representation of the multi-step synthesis of the esterase-responsive, albumin-binding BRD4 PROTAC (Alb-TAC #1). Reagents and conditions: (a) 5-azidovaleric acid, EDC, DMAP, CH<sub>2</sub>Cl<sub>2</sub>, RT, 1 h; (b) BCN-PEG<sub>2</sub>-Mal, DMF, RT, 1 h.

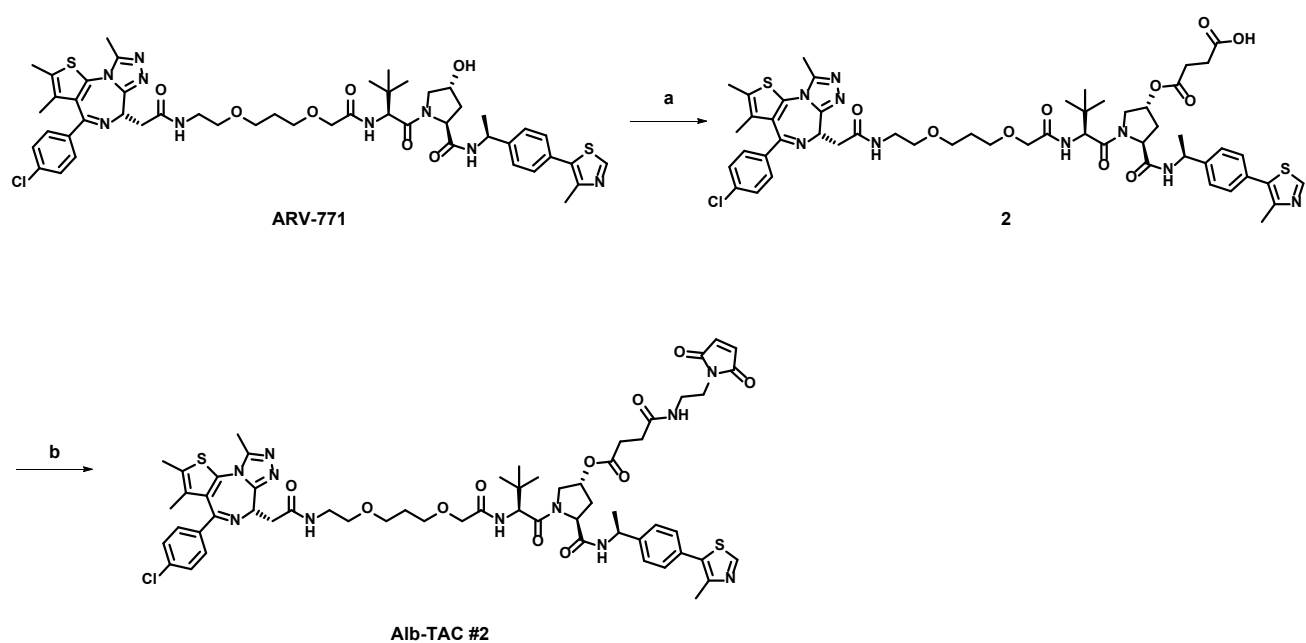


**Figure S2. Synthetic scheme of Alb-TAC #2.** Schematic representation of the multi-step synthesis of the Alb-TAC #2. Reagents and conditions: (a) succinic acid, EDC, DMAP, CH<sub>2</sub>Cl<sub>2</sub>, THF, RT, 1 h; (b) N-(2-aminoethyl)maleimide, HATU, DIPEA, DMF, RT, 1 h.

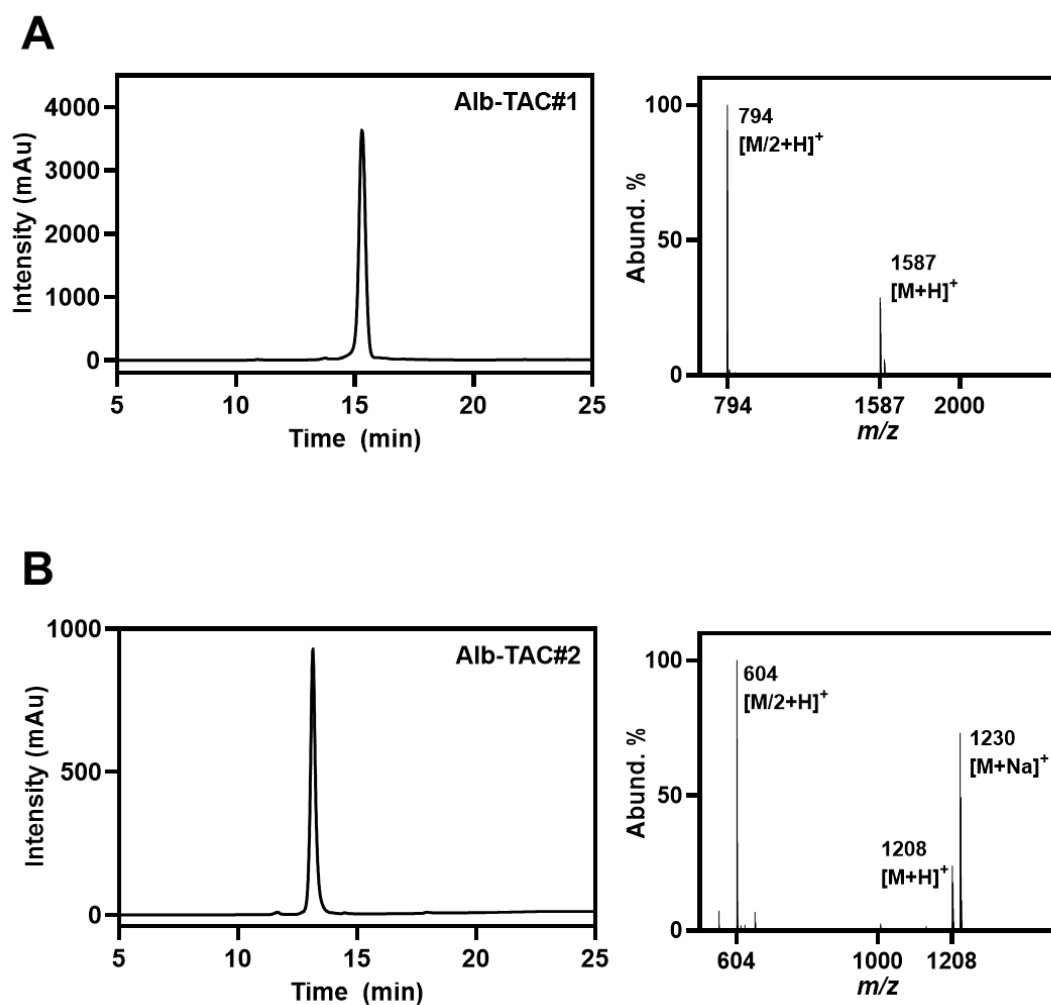


**Figure S3. Characterization of Alb-TACs.** (A) Analytical HPLC chromatogram and LC-MS spectra of (a) Alb-TAC#1 ( $m/z$  1587  $[M + H]^+$  and 794  $[M+2H]^{2+}$ ) and (B) Alb-TAC#2 ( $m/z$  1208  $[M + H]^+$ , 1230  $[M + Na]^+$  and 604  $[M+2H]^{2+}$ ). The presence of a single sharp peak and the observed mass confirm the high purity and identity of the synthesized conjugates.

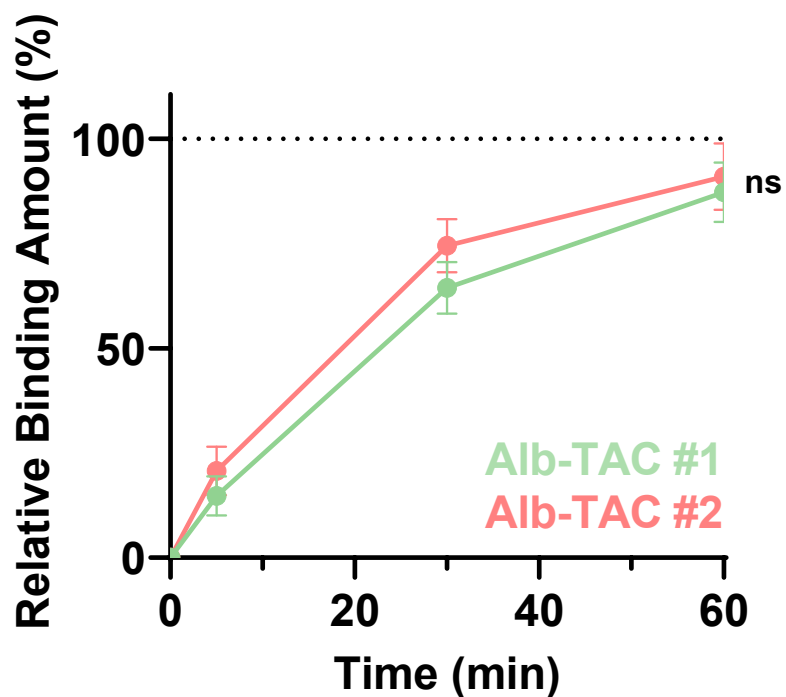


**Figure S4. Quantitative evaluation of albumin-binding kinetics.** Time-dependent relative binding amounts of Alb-TAC#1 and Alb-TAC#2. Each Alb-TAC (70  $\mu$ M) was incubated with serum albumin (100  $\mu$ M) in saline at 37  $^{\circ}$ C with constant stirring. The binding percentage was quantified based on the decrease in free Alb-TACs peak areas observed *via* HPLC. Data are presented as mean  $\pm$  SD. Statistical significance was determined by Student's t-test (ns, no significant).

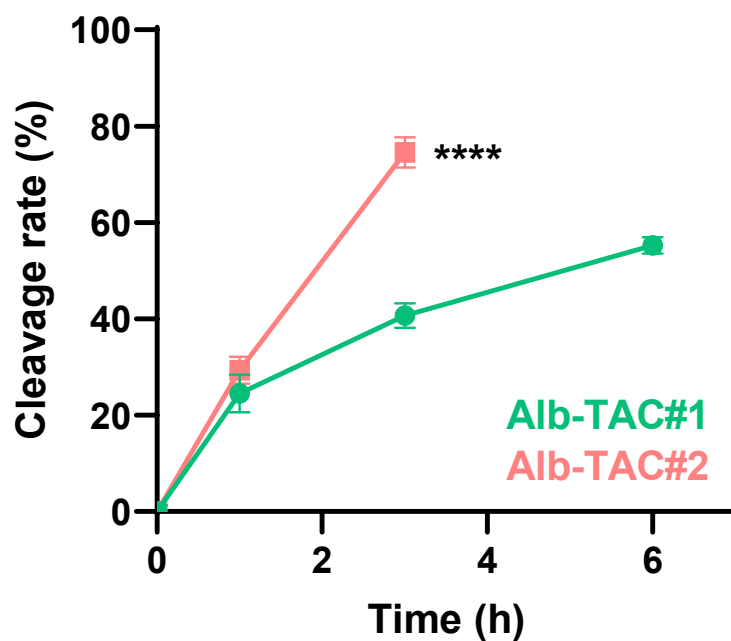


**Figure S5. Quantitative cumulative hydrolysis profiles of Alb-TACs.** Quantitative cumulative hydrolysis profiles of Alb-TAC#1 and Alb-TAC#2 over 12 h of incubation with esterase (30 U/mL) at 37 °C. The percentage of hydrolysis was calculated by quantifying the peak area of the released ARV-771 relative to the initial Alb-TAC peak using RP-HPLC. Data are presented as mean ± SD. Statistical significance was determined by Student's t-test (\*\*\*\* $p < 0.0001$ ).

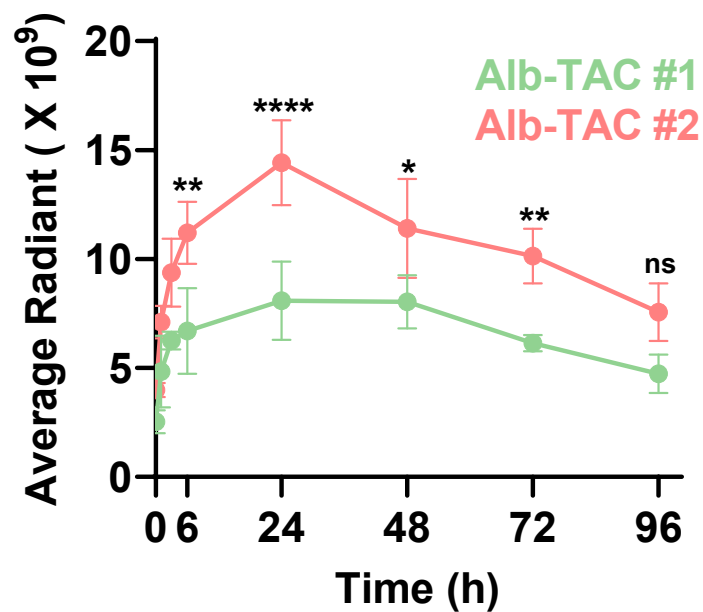


**Figure S6. Quantitative analysis of *in vivo* biodistribution of Alb-TAC #1 and Alb-TAC #2.**

Time-dependent fluorescence intensity profiles of tumor regions obtained from NIRF imaging (Figure 1G) following intravenous administration of Cy5.5-labeled Alb-TAC #1 or Alb-TAC #2 (10 mg/kg) in CT26 tumor-bearing mice ( $n = 3$  per group). Fluorescence intensities were quantified from tumor-localized regions of interest (ROIs) at each time point. Data are presented as mean  $\pm$  SD. Statistical significance was determined by two-way ANOVA with Tukey's post-hoc test for (B) (ns, not significant; \* $p < 0.05$ ; \*\* $p < 0.01$ ; \*\*\*\* $p < 0.0001$ ).

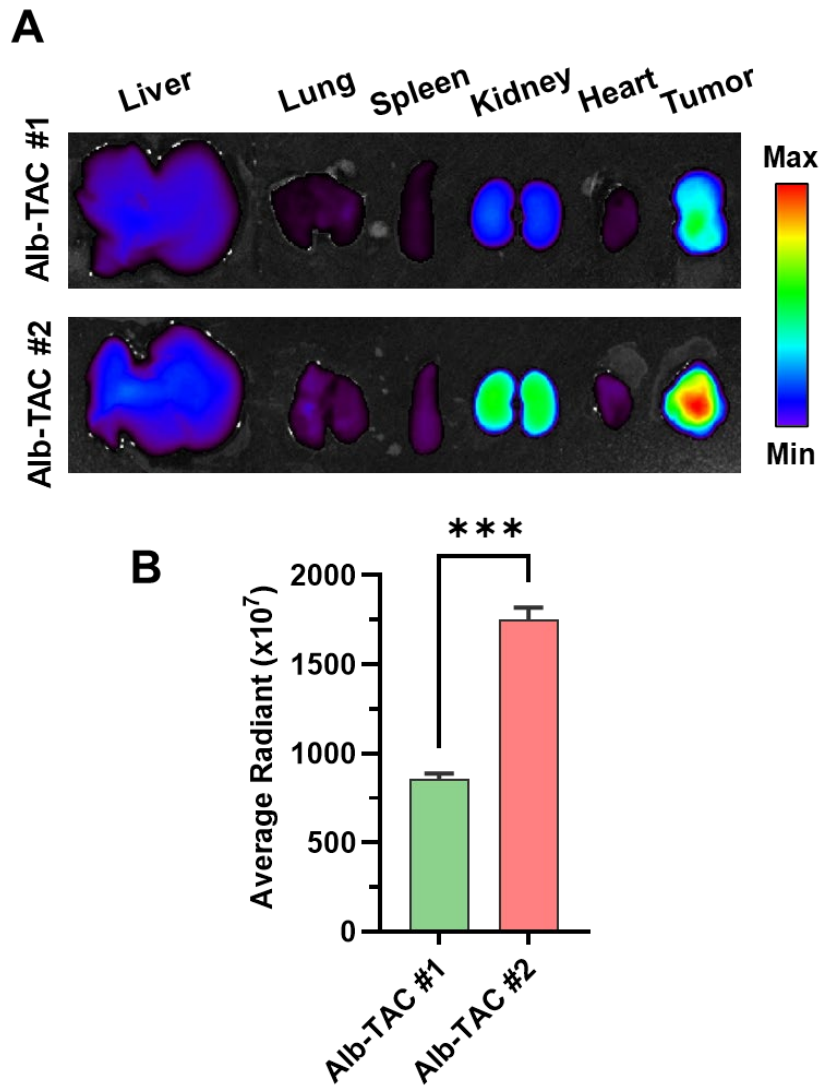


**Figure S7. *Ex vivo* biodistribution analysis of Cy5.5-labeled Alb-TAC #1 and Alb-TAC #2.** (A) Fluorescence images of major organs (liver, lung, spleen, kidney, and heart) and tumor tissues collected 24 h after intravenous injection of Cy5.5-labeled Alb-TAC #1 or Alb-TAC #2 (10 mg/kg) in CT26 tumor-bearing mice (n = 3 per group). (B) Quantification of tumor-associated fluorescence signals shown in (A), derived from *ex vivo* imaging of excised tumors collected 24 h post-injection. Data are presented as mean  $\pm$  SD. Statistical significance was determined by Student's t-test (\*\*\*)  $p < 0.001$ ).

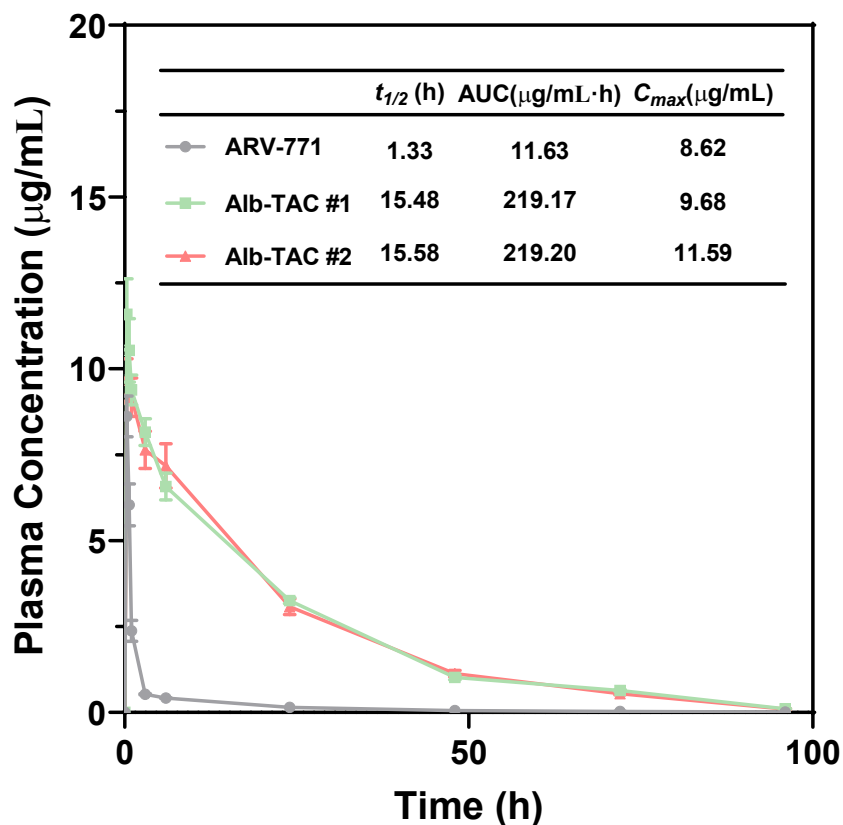


**Figure S8.** *In vivo* pharmacokinetic profiles of Alb-TACs in normal mice. Plasma concentration-time curves of Cy5.5-conjugated ARV-771 (10 mg/kg, equiv. to ARV-771), Cy5.5-conjugated Alb-TAC#1 (10 mg/kg, equiv. to ARV-771), and Cy5.5-conjugated Alb-TAC#2 (10 mg/kg, equiv. to ARV-771) following a single intravenous injection in BALB/c mice. The inserted table summarizing key pharmacokinetic parameters, including half-life ( $t_{1/2}$ ), area under the curve (AUC), and maximum plasma concentration ( $C_{max}$ ). Data represent mean  $\pm$  SD (n = 3).

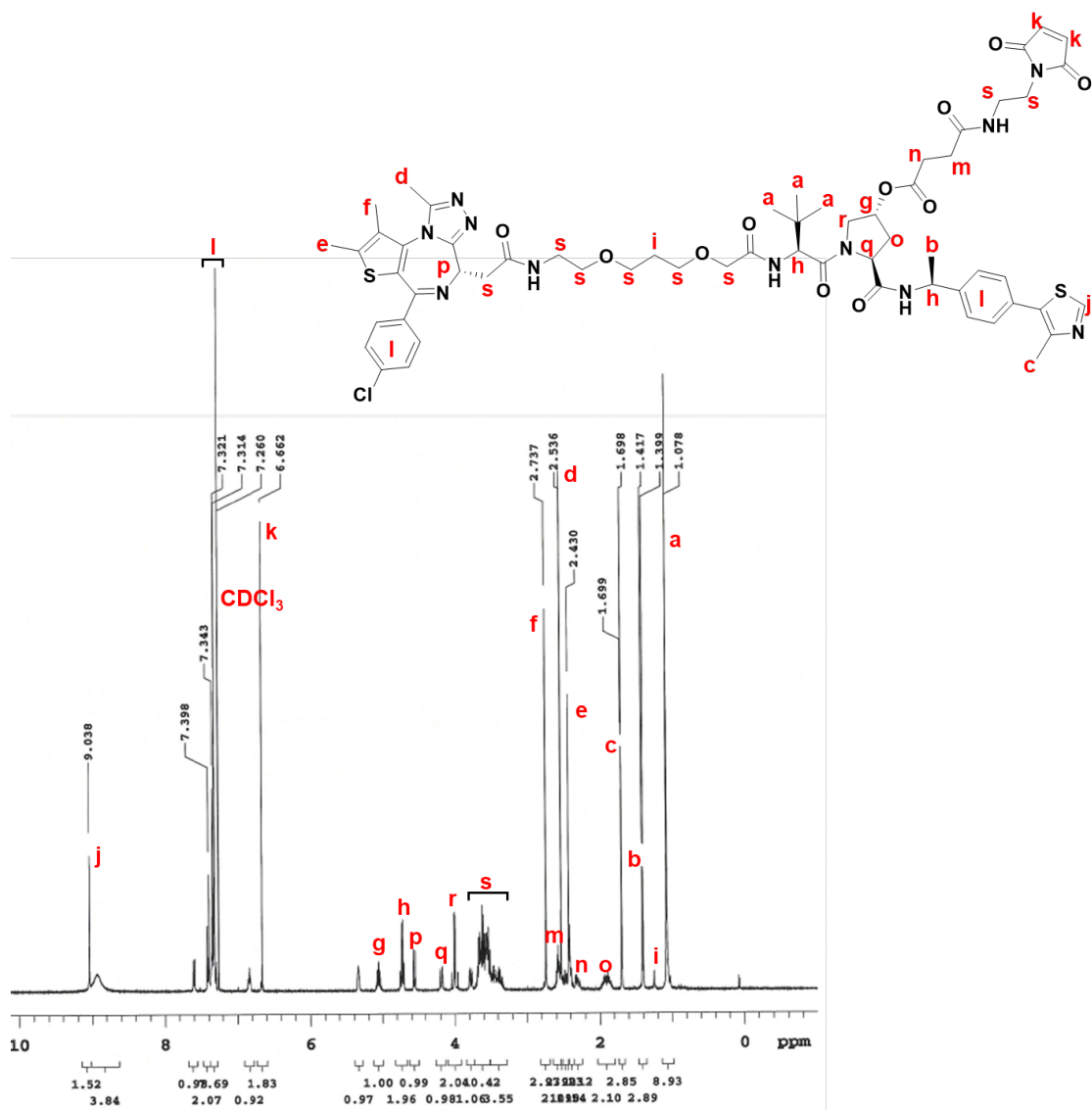


**Figure S9. <sup>1</sup>H NMR spectrum of Alb-TAC#2.** <sup>1</sup>H NMR (600 MHz) spectrum of Alb-TAC#2 measured in CDCl<sub>3</sub> (10 mg/mL). The chemical structure is labeled with letters corresponding to the assigned peaks in the spectrum.

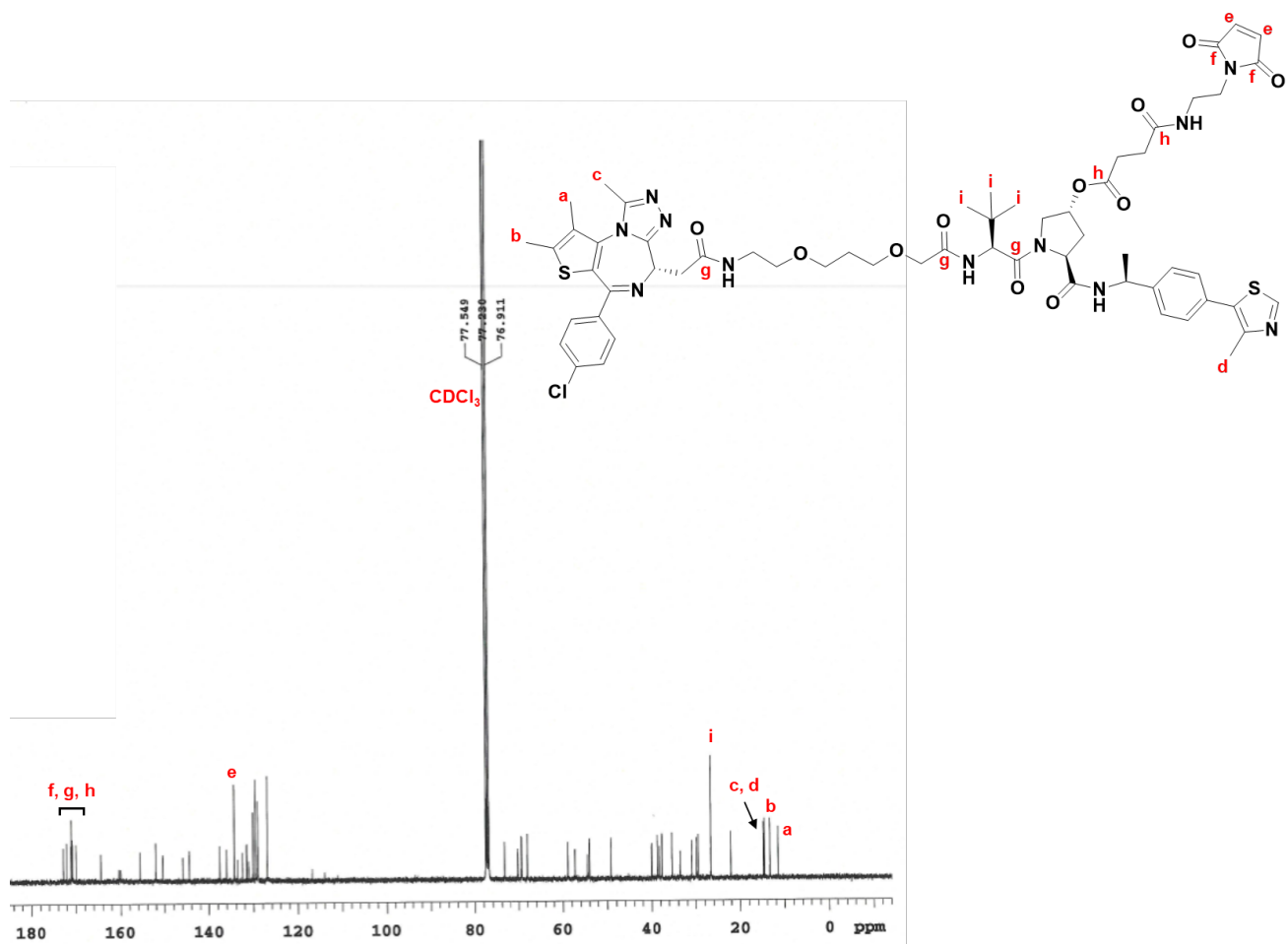


**Figure S10.  $^{13}\text{C}$  NMR spectrum of Alb-TAC#2.**  $^{13}\text{C}$  NMR (600 MHz) spectrum of Alb-TAC#2 measured in  $\text{CDCl}_3$  (10 mg/mL). The chemical structure is labeled with letters corresponding to the assigned peaks in the spectrum.

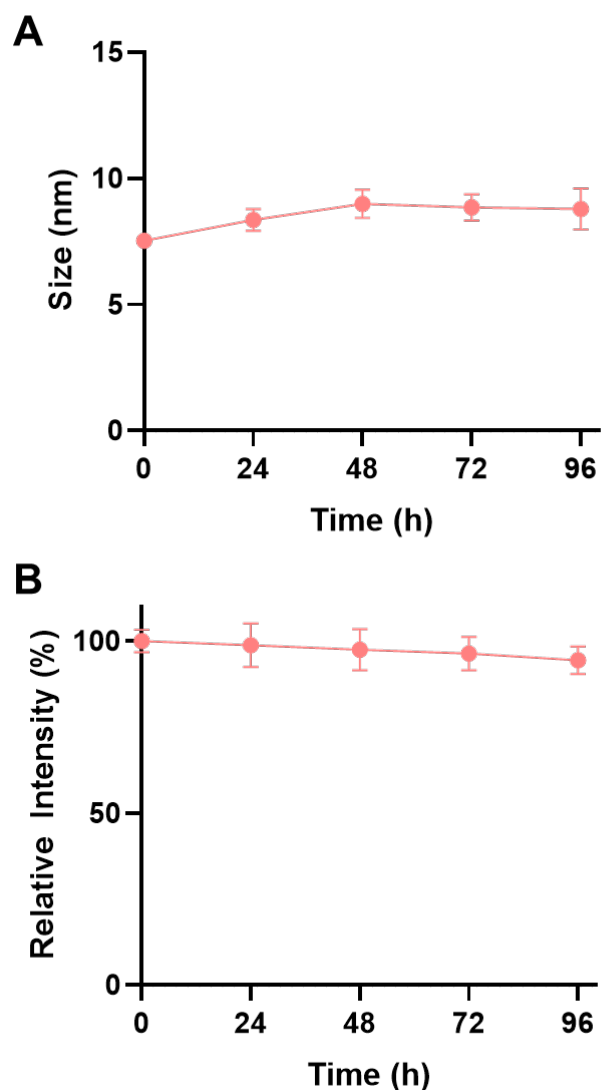


**Figure S11. Long-term stability of Alb-TAC in mouse serum.** (A) Hydrodynamic size distribution of Alb-TAC measured by DLS during incubation in mouse serum at 37 °C for 96 h. (B) LC-MS analysis of Alb-TAC purity, expressed as the percentage of Alb-TAC peak area relative to total peak area, in mouse serum at 37 °C over 96 h.

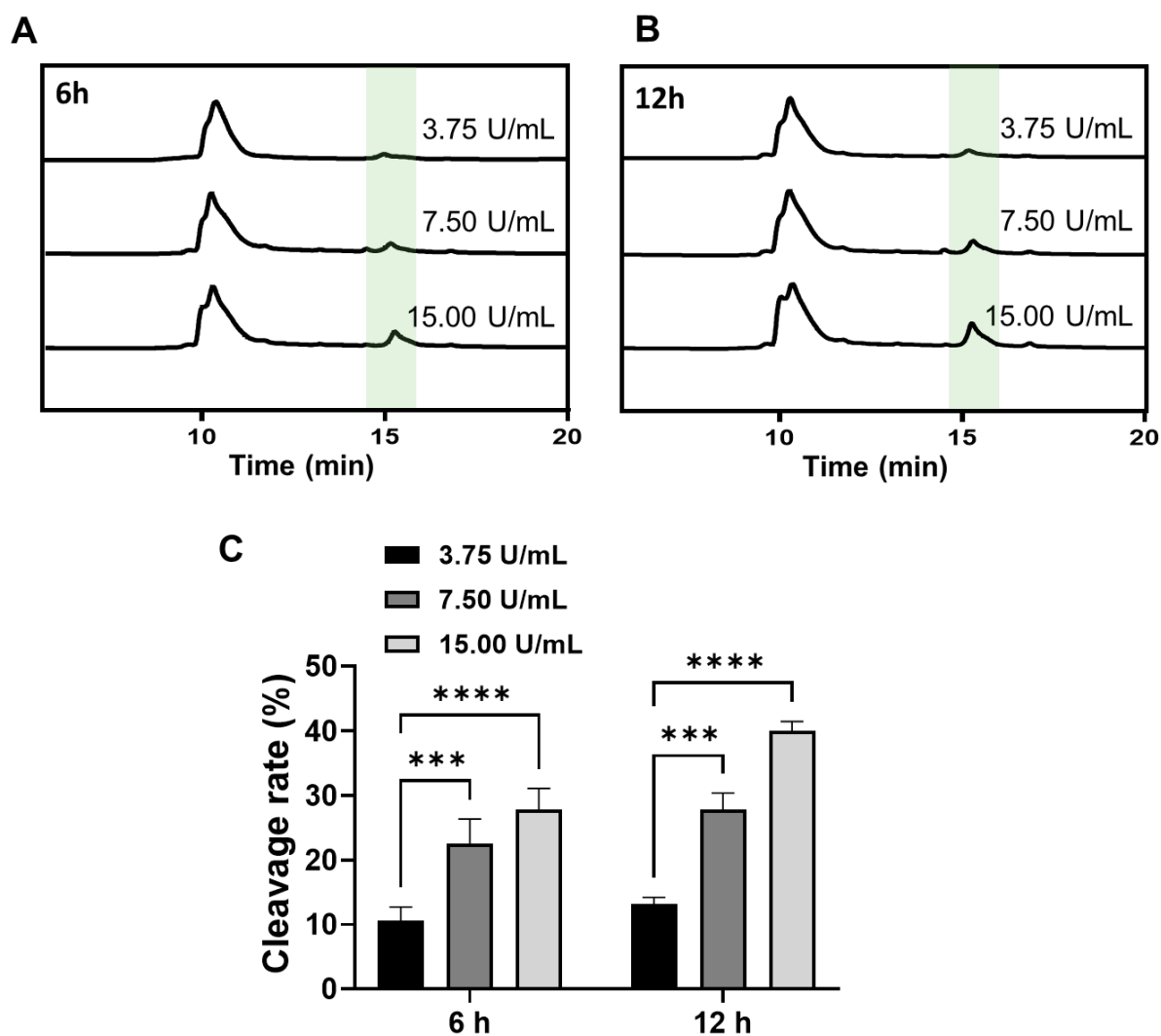


**Figure S12. Esterase concentration-dependent cleavage and release kinetics of Alb-TAC.** (A, B) RP-HPLC chromatograms of Alb-TAC following incubation with varying concentrations of esterase (3.75, 7.50, and 15.00 U/mL) for 6 h and 12 h. The shaded green area indicates the peak corresponding to released ARV-771. (C) Quantitative analysis of Alb-TAC cleavage rate (%) as a function of esterase concentration and incubation time, calculated as the peak area of released ARV-771 relative to total peak area. Data are presented as mean  $\pm$  SD. Statistical significance was determined by two-way ANOVA with Tukey's post-hoc test for (C) (\*\*\*)  $p < 0.001$ ; \*\*\*\*)  $p < 0.0001$ .

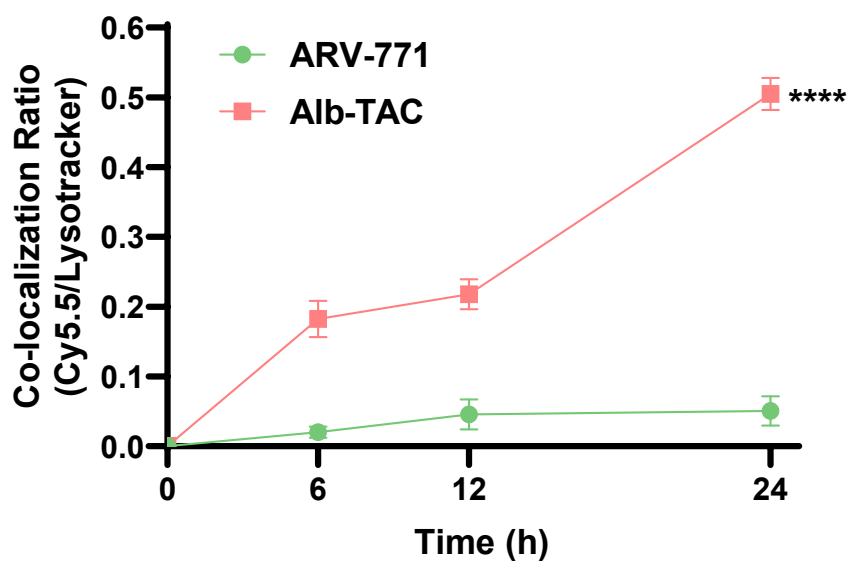


**Figure S13. Quantitative co-localization analysis of Alb-TAC with LysoTracker.** Quantitative co-localization analysis of Cy5.5-labeled ARV-771 and Cy5.5-labeled Alb-TAC with LysoTracker in CT26 cells, expressed as co-localization ratio over 24 h. Data are presented as mean  $\pm$  SD. Statistical significance was determined by Student's t-test (\*\*\*\* $p < 0.0001$ ).

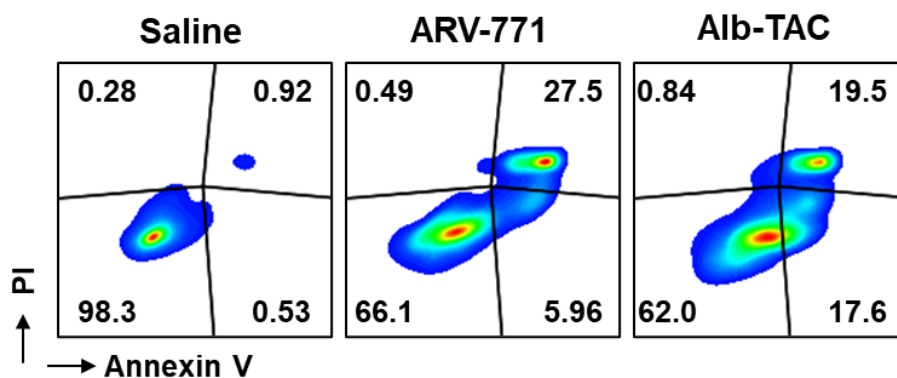


**Figure S14. Flow cytometric analysis of cell death mode induced by Alb-TAC.** Representative flow cytometry scatter plots of CT26 cells stained with Annexin V-FITC and PI after 48 h of treatment with 5  $\mu$ M ARV-771 or 5  $\mu$ M Alb-TAC. The quadrants represent viable (Annexin V<sup>-</sup>/PI<sup>-</sup>), early apoptotic (Annexin V<sup>+</sup>/PI<sup>-</sup>), and late apoptotic/necrotic (Annexin V<sup>+</sup>/PI<sup>+</sup>) cell populations. Data are presented as mean  $\pm$  SD (n = 3).

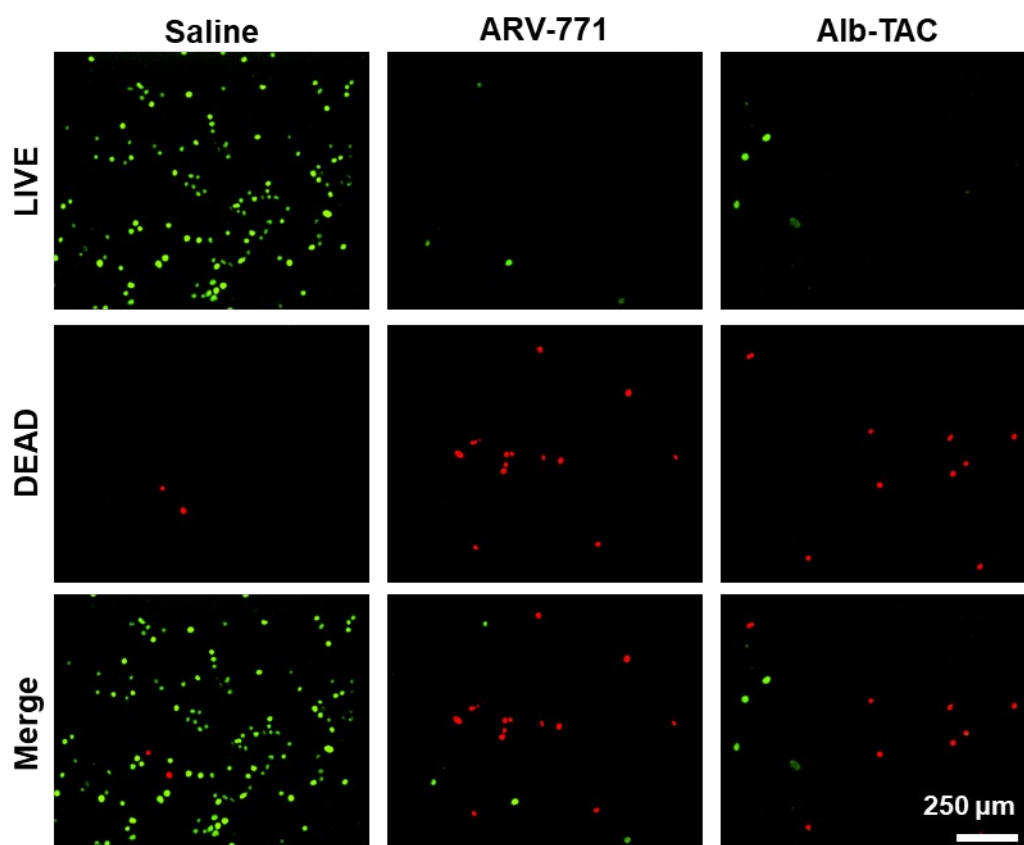


**Figure S15. Results of live/dead viability assay of CT26 cells treated with Alb-TAC and ARV-771.** Representative fluorescence microscopy images of CT26 cells treated with 5  $\mu$ M ARV-771 or Alb-TAC for 48 h, followed by staining with calcein-AM (live, green) and 7-aminoactinomycin D (7-AAD; dead, red) (scale bar, 250  $\mu$ m).

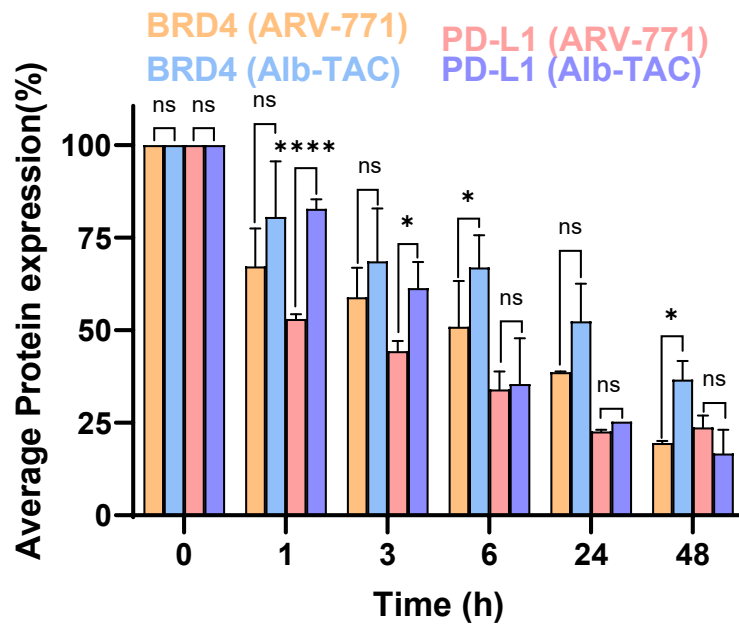


**Figure S16. Quantitative analysis of BRD4 and PD-L1 band intensities from Figure 3C.**

Western blot analysis of CT26 cells treated with 10  $\mu$ M ARV-771 or Alb-TAC for different incubation times (0, 1, 3, 6, 24, and 48 h) to assess time-dependent degradation kinetics of BRD4 and its downstream proteins (PD-L1, c-Myc, and Bcl-2). Data are presented as mean  $\pm$  SD. Statistical significance was determined by two-way ANOVA with Tukey's post-hoc test (ns, not significant; \* $p$  < 0.05; \*\*\*\* $p$  < 0.0001).

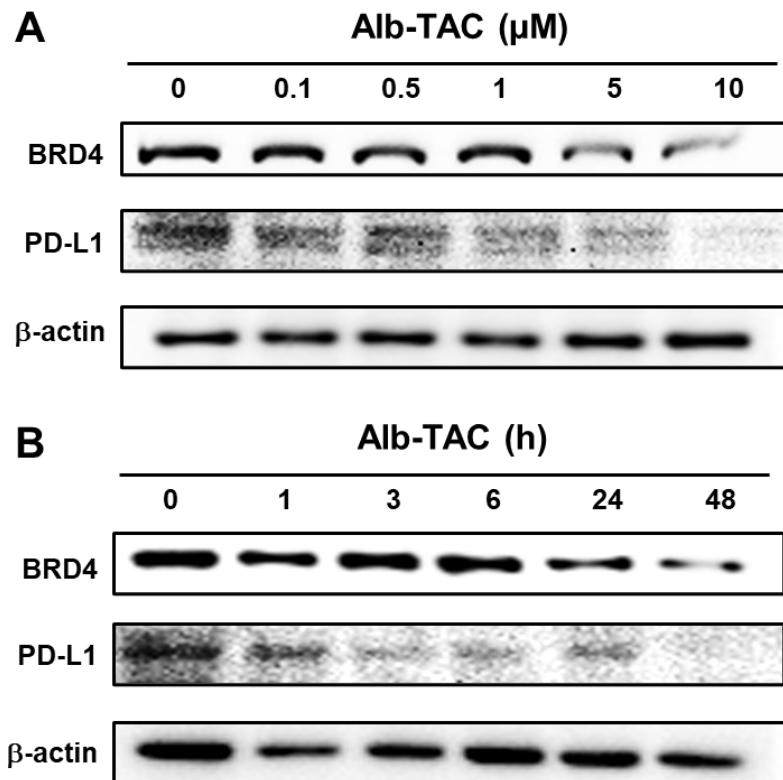


**Figure S17. *In vitro* BRD4 and PD-L1 degradation of Alb-TAC in 4T1 murine mammary carcinoma model.** (A) Western blot analysis of 4T1 cells treated with increasing concentrations (0, 0.1, 0.5, 1, 5, and 10  $\mu\text{M}$ ) of Alb-TAC for 24 h to evaluate BRD4 and PD-L1 degradation. (B) Western blot analysis of 4T1 cells treated with 10  $\mu\text{M}$  Alb-TAC for different incubation times (0, 1, 3, 6, 24, and 48 h) to assess time-dependent degradation kinetics of BRD4 and PD-L1.

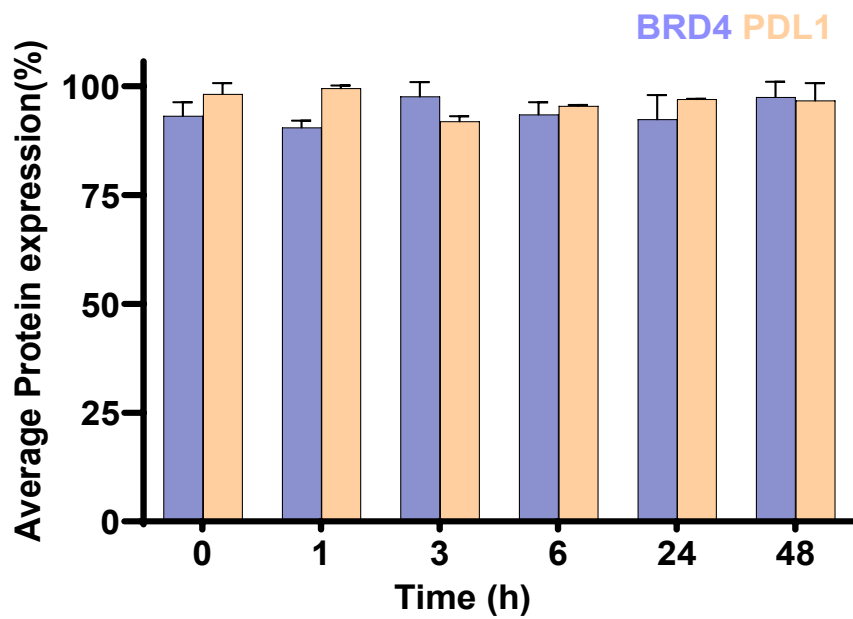


**Figure S18. Quantitative analysis of BRD4 and PD-L1 band intensities from Figure 3D.**

Western blot analysis of CT26 cells co-treated with Alb-TAC (10  $\mu$ M) and the VHL inhibitor VH298 to verify VHL-dependent BRD4 degradation over time.

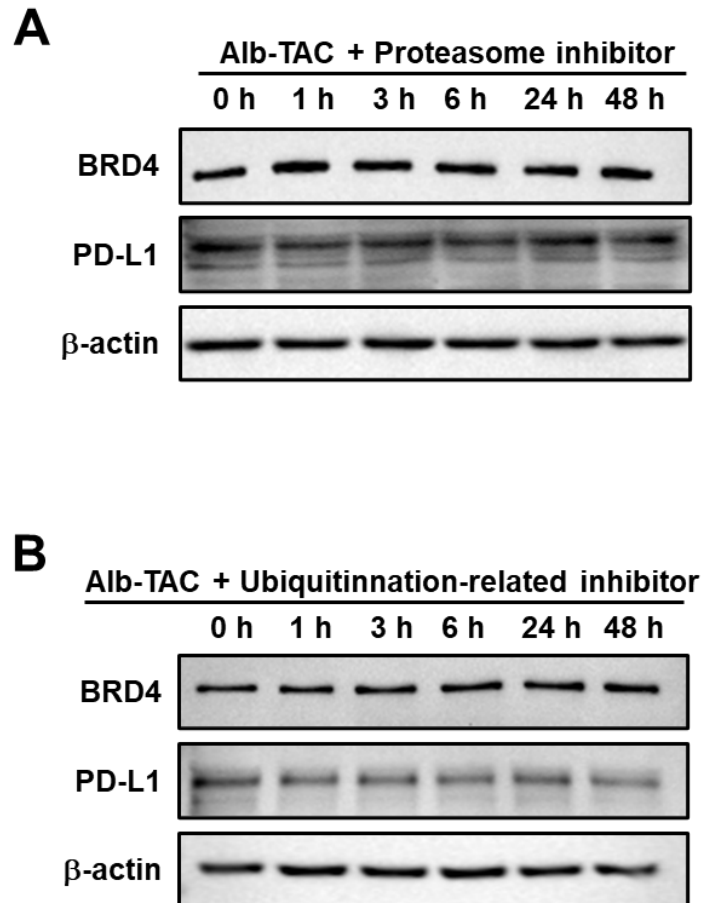


**Figure S19. Confirmation of the ubiquitin-proteasome-dependent degradation pathway of Alb-TAC.** Western blot analysis of BRD4 and PD-L1 levels in CT26 cells co-treated with Alb-TAC and (A) NAE inhibitor Pevonedistat (5  $\mu$ M) or (B) proteasome inhibitor Bortezomib (10 nM) over 48 h.

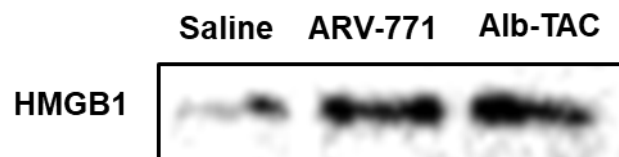


**Figure S20. Western blot analysis of extracellular HMGB1 release following Alb-TAC treatment.** Representative Western blot of HMGB1 levels in culture supernatants collected from CT26 cells treated with 10  $\mu$ M ARV-771 or 10  $\mu$ M Alb-TAC for 24 h.

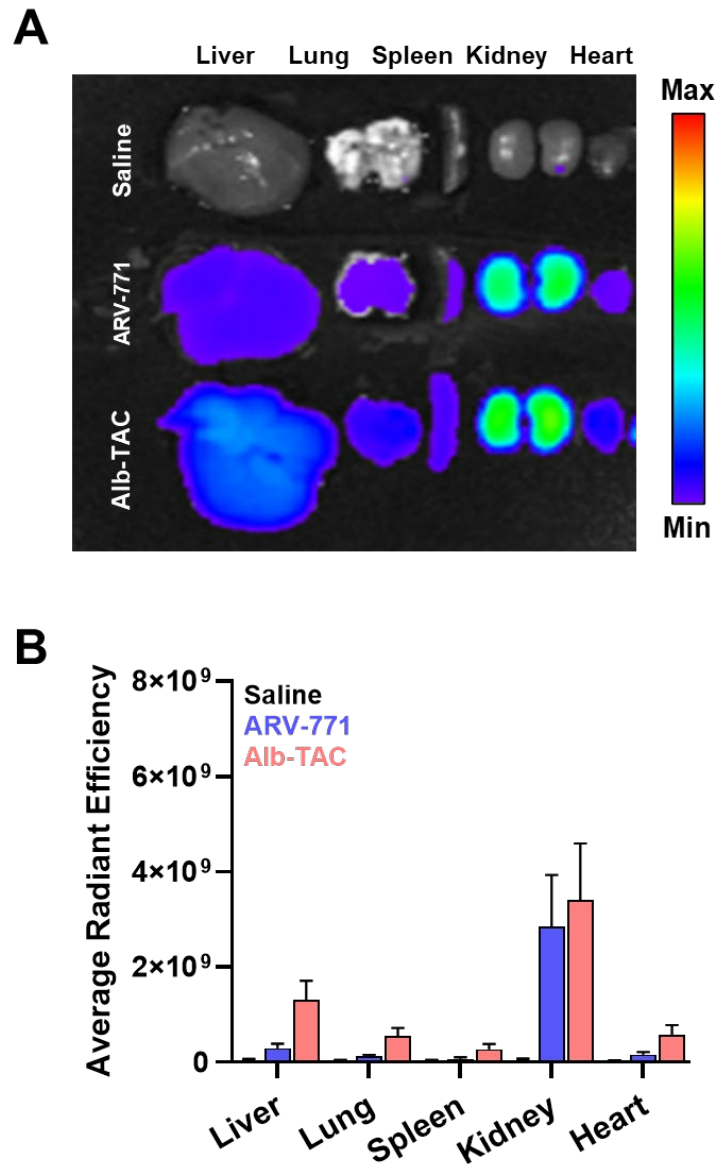


**Figure S21. *Ex vivo* biodistribution of Cy5.5-labeled ARV-771 and Alb-TAC in CT26 tumor-bearing mice.** (A) Representative *ex vivo* near-infrared fluorescence (NIRF) images of major organs (liver, lung, spleen, kidney, and heart) collected 24 h after intravenous injection of Cy5.5-labeled ARV-771 or Cy5.5-labeled Alb-TAC (3 mg/kg; n = 3 per group). (B) Quantitative analysis of fluorescence intensity of major organs.

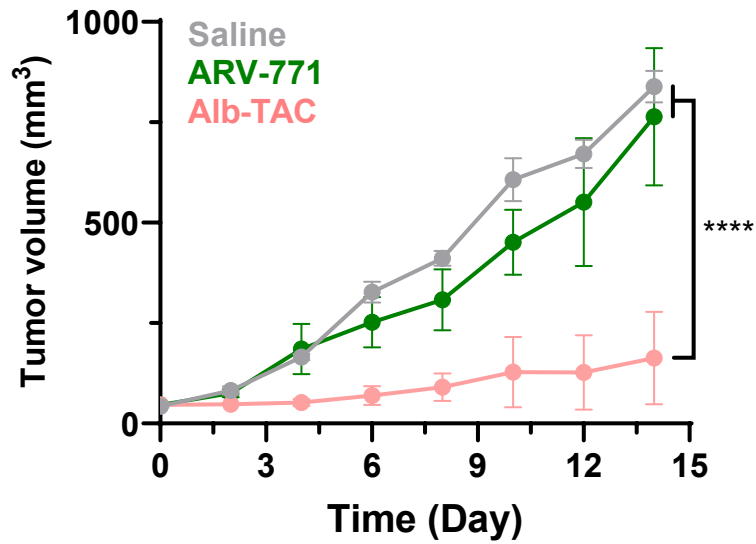


**Figure S22. *In vivo* anti-tumor efficacy of Alb-TAC in 4T1 murine mammary carcinoma model.** Tumor growth curves of 4T1 tumor-bearing mice treated intravenously with saline, ARV-771 (10 mg/kg), or Alb-TAC (10 mg/kg, equiv. to ARV-771) every three days for four doses (days 0, 3, 6, 9 and 12). Data are presented as mean  $\pm$  SD. Statistical significance was determined by two-way ANOVA with Tukey's post-hoc test (\*\*\*\* $p < 0.0001$ ).

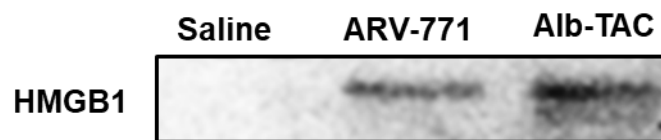


**Figure S23. Western blot analysis of HMGB1 expression in tumor tissues following Alb-TAC treatment.** Representative Western blot of HMGB1 levels in tumor lysates collected from CT26 tumor-bearing mice treated with saline (control), ARV-771 (10 mg/kg), or Alb-TAC (10 mg/kg) for 7 days.

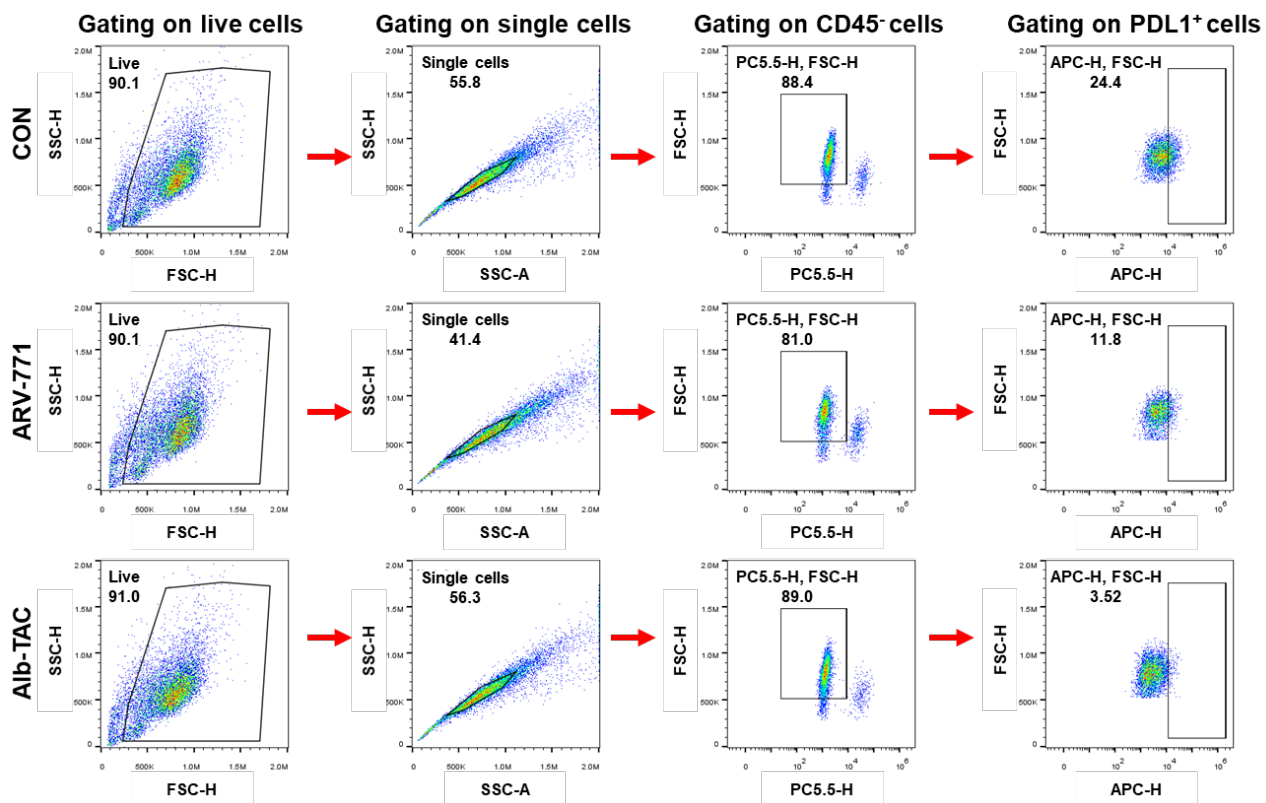


**Figure S24. Gating strategy for PD-L1-expressing immune cells.** Representative flow cytometry plots illustrating the gating sequence for PD-L1 expression on tumor cells.

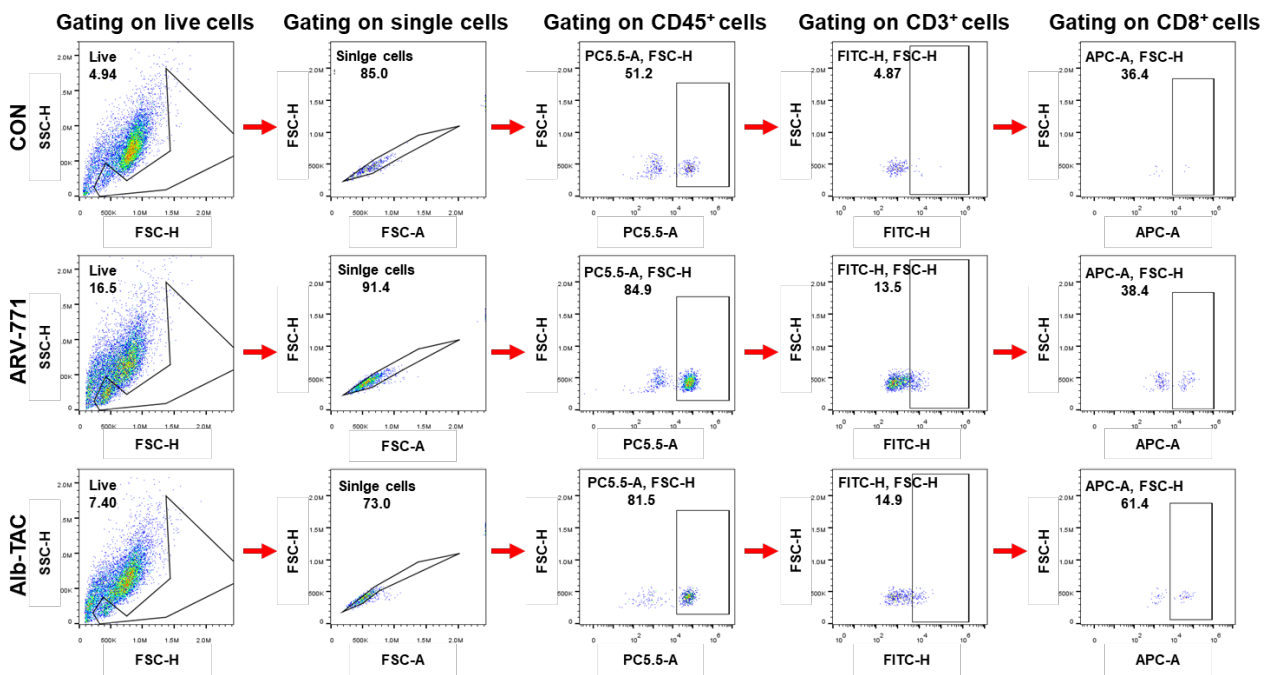


**Figure S25. Gating strategy for CD8<sup>+</sup> T cells.** Representative flow cytometry plots illustrating the gating sequence for CD8<sup>+</sup> expression on T cell subsets.

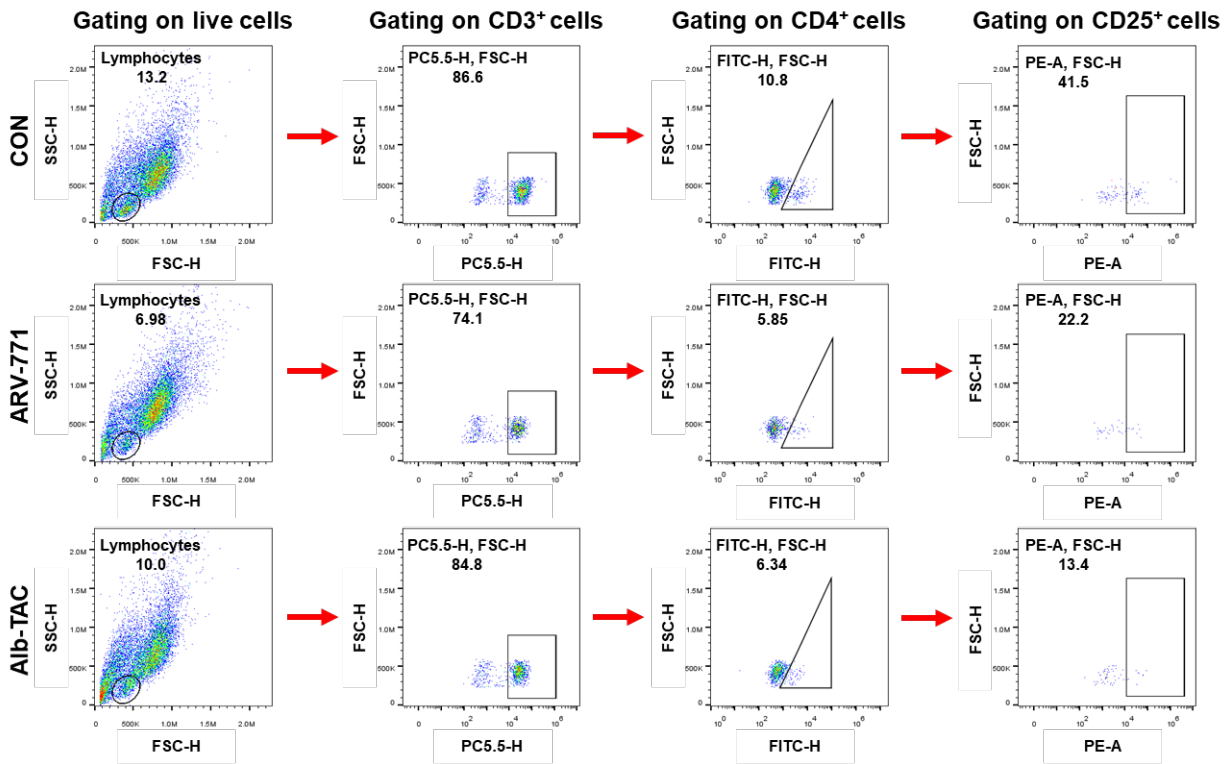


**Figure S26. Gating strategy for regulatory T cells.** Representative flow cytometry plots illustrating the gating sequence for CD25<sup>+</sup> expression on T cell subsets.

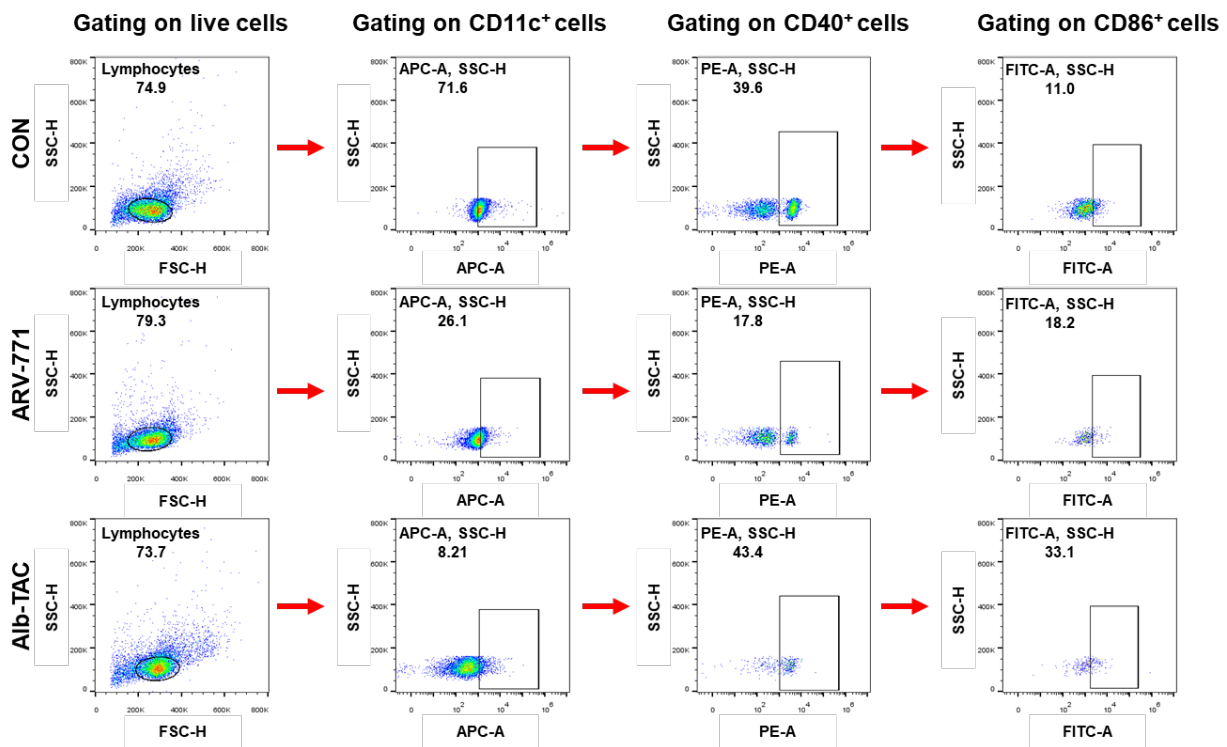


**Figure S27. Gating strategy for mature dendritic cells (DCs).** Representative flow cytometry plots illustrating the gating sequence for CD86<sup>+</sup> expression on DC subsets.

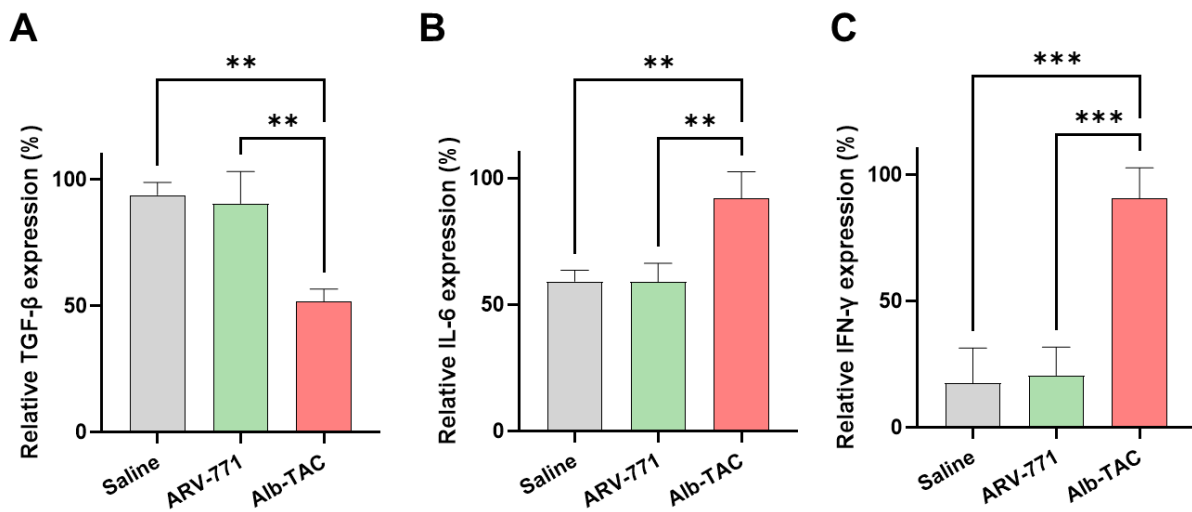


**Figure S28. Functional cytokine profiling within the TME.** Relative expression levels of (A) TGF-β, (B) IL-6, and (C) IFN-γ in the plasma of CT26 tumor-bearing mice. Data are presented as mean ± SD (n = 3). Statistical significance was determined by one-way ANOVA with Tukey's post-hoc test for (C, D) (\*\* $p < 0.01$ ; \*\*\* $p < 0.001$ ).

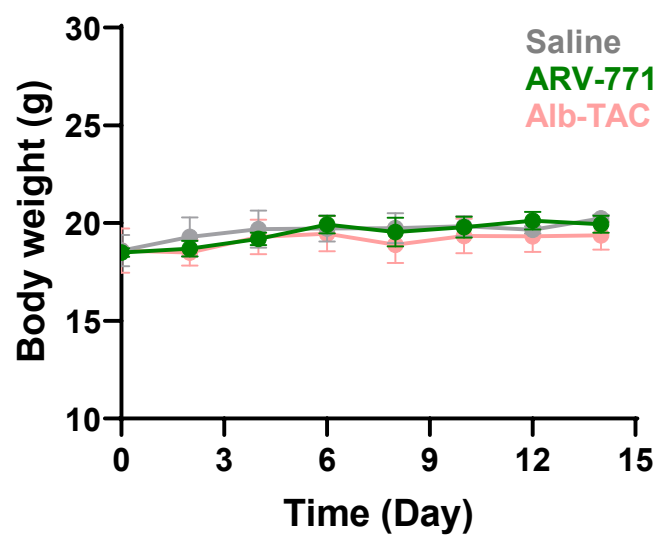


**Figure S29.** *In vivo* safety of Alb-TAC in 4T1 murine mammary carcinoma model. Body weight changes of 4T1 tumor-bearing mice treated intravenously with saline, ARV-771 (10 mg/kg), or Alb-TAC (10 mg/kg, equiv. to ARV-771) every three days for four doses (days 0, 3, 6, 9 and 12).

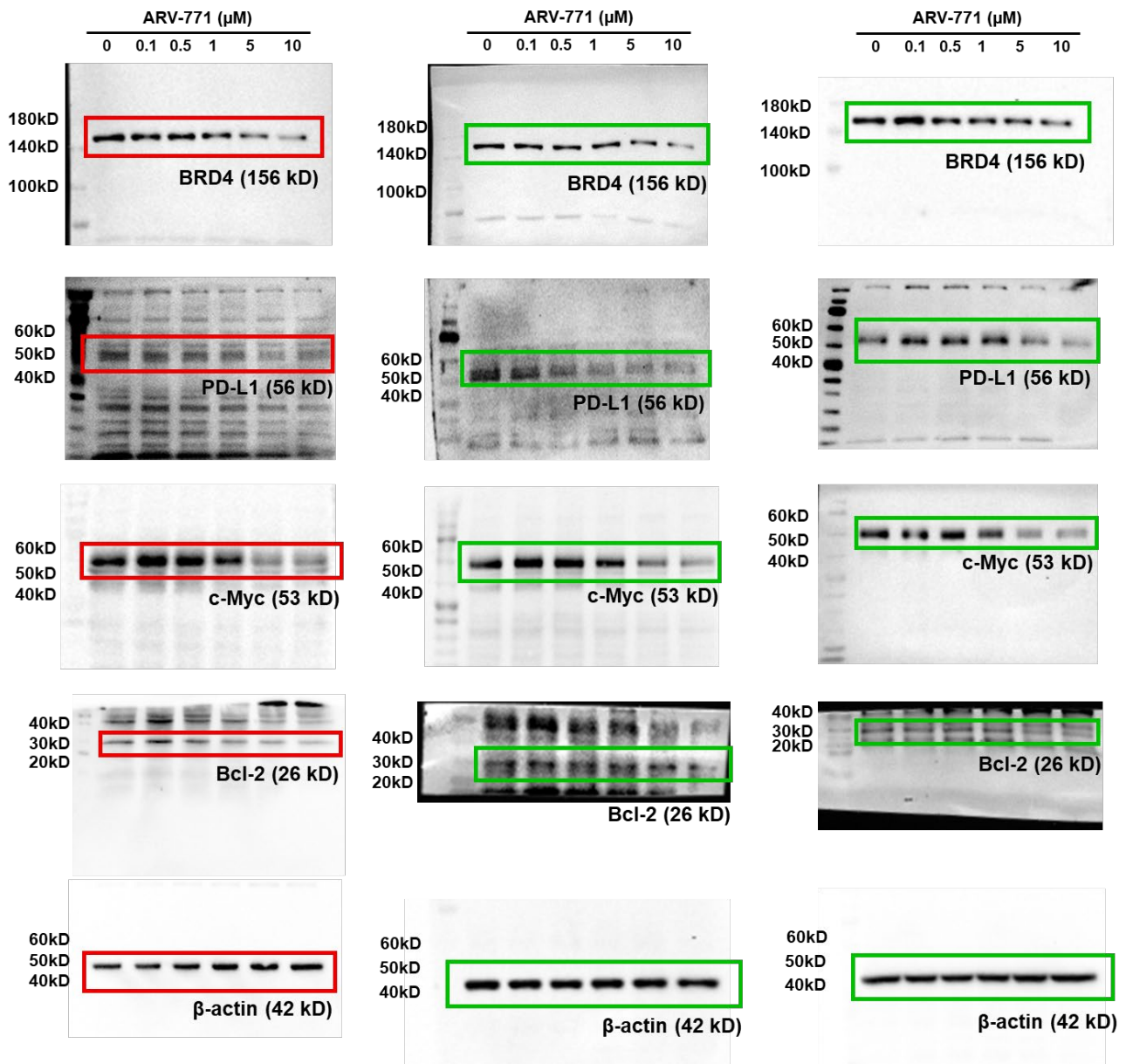


**Figure S30. Uncropped western blot results of ARV-771-treated samples in Figure 3A.** Western blot analysis of CT26 cells treated with increasing concentrations (0, 0.1, 0.5, 1, 5, and 10  $\mu\text{M}$ ) of ARV-771 for 24 h to evaluate BRD4, PD-L1, c-Myc, Bcl-2, and  $\beta$ -actin protein levels. Red boxes indicate the cropped regions presented in Figure 3A. Green boxes indicate the remaining two independent biological replicates. All data represent three independent biological replicates.

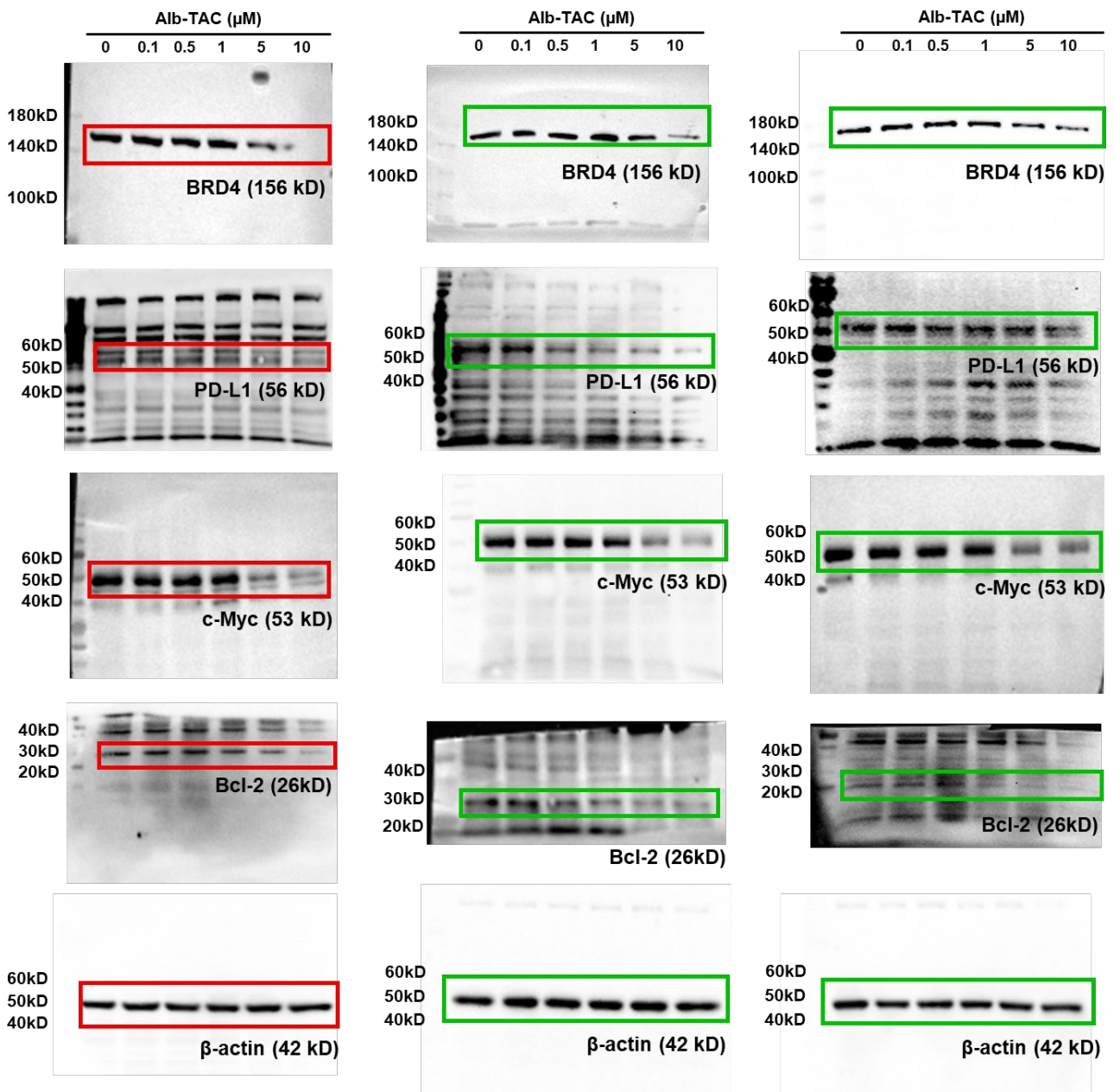


**Figure S31. Uncropped western blot results of Alb-TAC-treated samples in Figure 3A.** Western blot analysis of CT26 cells treated with increasing concentrations (0, 0.1, 0.5, 1, 5, and 10  $\mu\text{M}$ ) of Alb-TAC for 24 h to evaluate BRD4, PD-L1, c-Myc, Bcl-2, and  $\beta$ -actin protein levels. Red boxes indicate the cropped regions presented in **Figure 3A**. Green boxes indicate the remaining two independent biological replicates. All data represent three independent biological replicates.

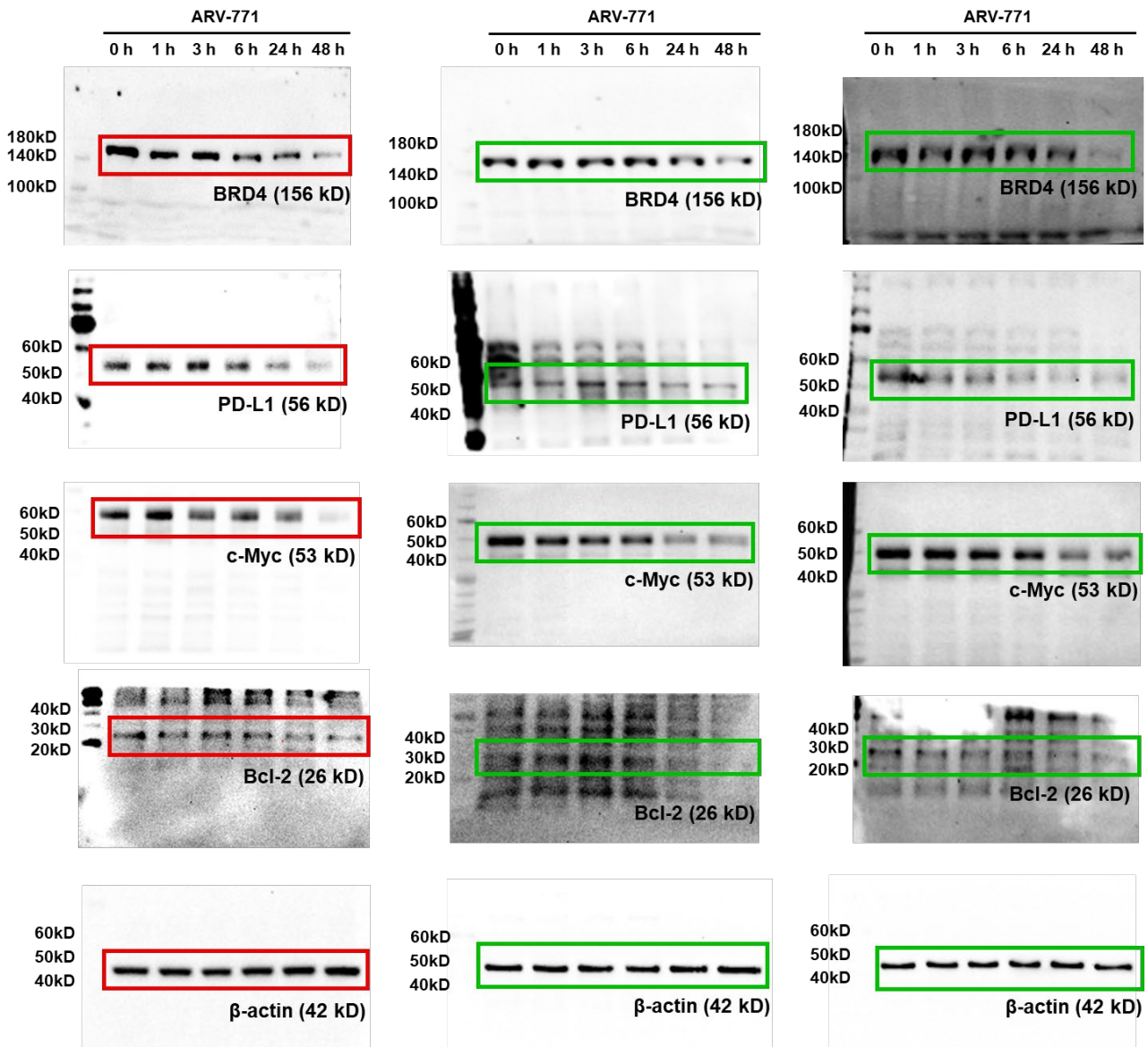


**Figure S32. Uncropped western blot results of ARV-771-treated samples in Figure 3C.** Western blot analysis of CT26 cells treated with 10  $\mu$ M ARV-771 for different incubation times (0, 1, 3, 6, 24, and 48 h) to evaluate BRD4, PD-L1, c-Myc, Bcl-2, and  $\beta$ -actin protein levels. Red boxes indicate the cropped regions presented in **Figure 3C**. Green boxes indicate the remaining two independent biological replicates. All data represent three independent biological replicates.

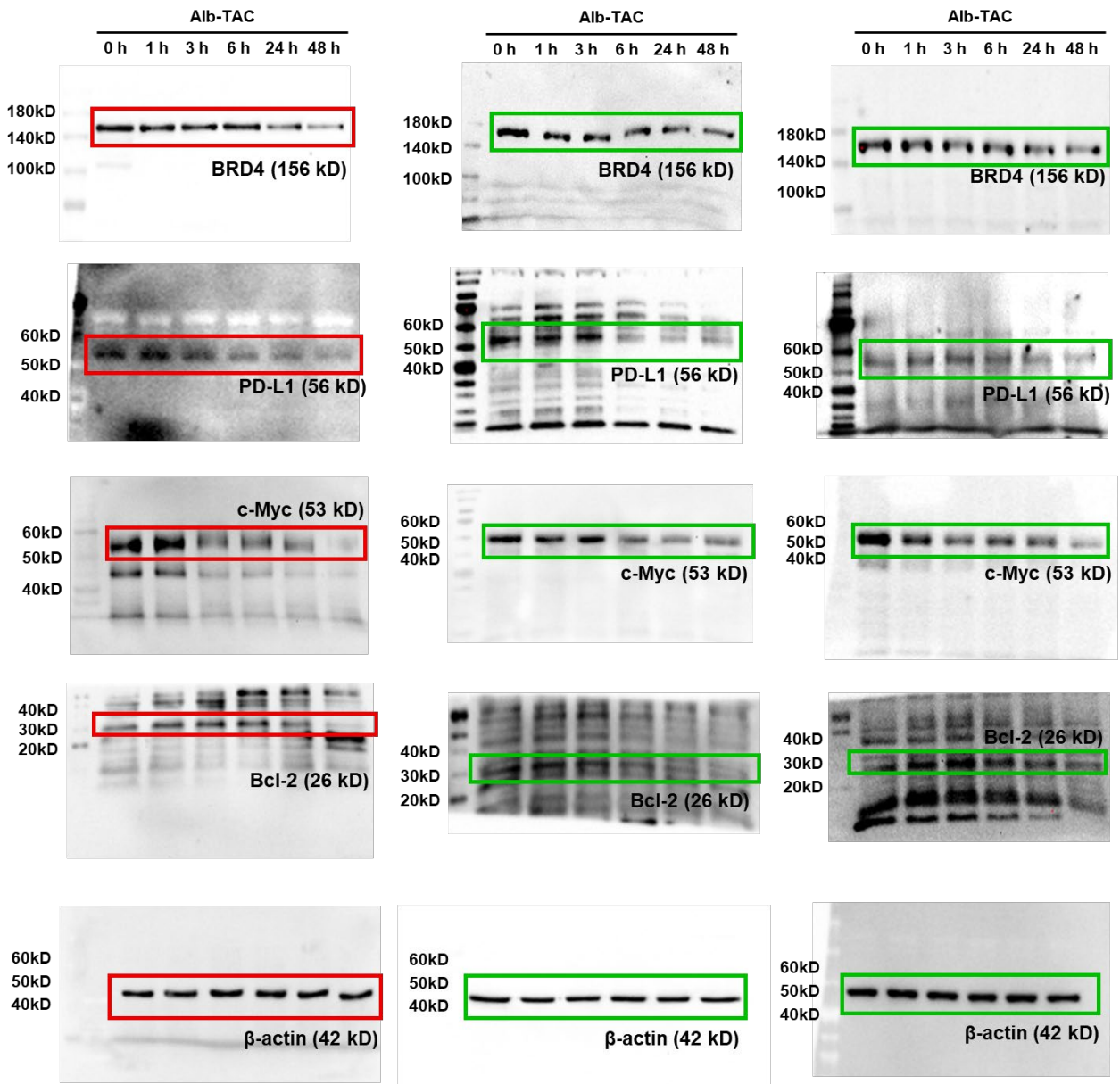


**Figure S33. Uncropped western blot results of Alb-TAC-treated samples in Figure 3C.** Western blot analysis of CT26 cells treated with 10  $\mu$ M Alb-TAC for different incubation times (0, 1, 3, 6, 24, and 48 h) to evaluate BRD4, PD-L1, c-Myc, Bcl-2, and  $\beta$ -actin protein levels. Red boxes indicate the cropped regions presented in **Figure 3C**. Green boxes indicate the remaining two independent biological replicates. All data represent three independent biological replicates.

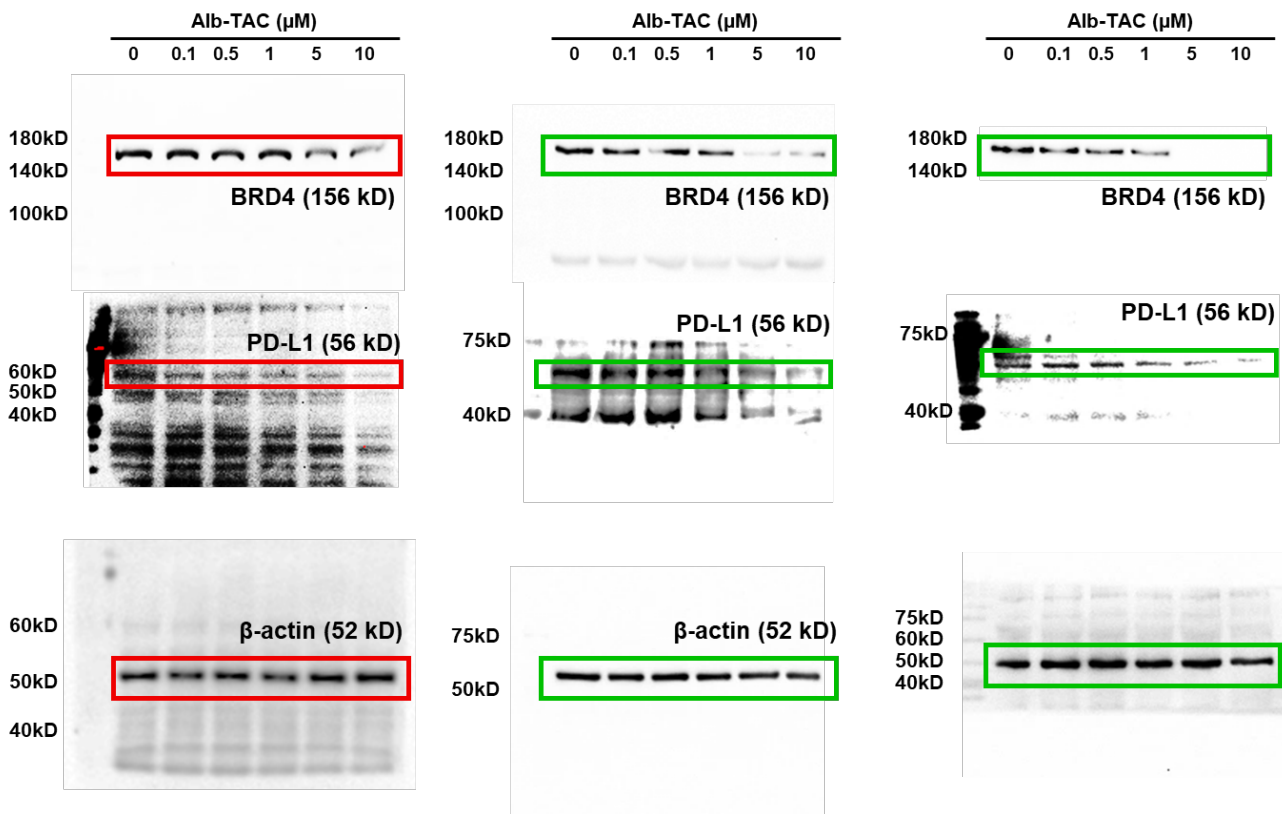


**Figure S34. Uncropped western blot results of Alb-TAC-treated samples in Figure S17A.**

Western blot analysis of 4T1 cells treated with increasing concentrations (0, 0.1, 0.5, 1, 5, and 10  $\mu$ M) of Alb-TAC for 24 h to evaluate BRD4, PD-L1, and  $\beta$ -actin protein levels. Red boxes indicate the cropped regions presented in **Figure S17A**. Green boxes indicate the remaining two independent biological replicates. All data represent three independent biological replicates.

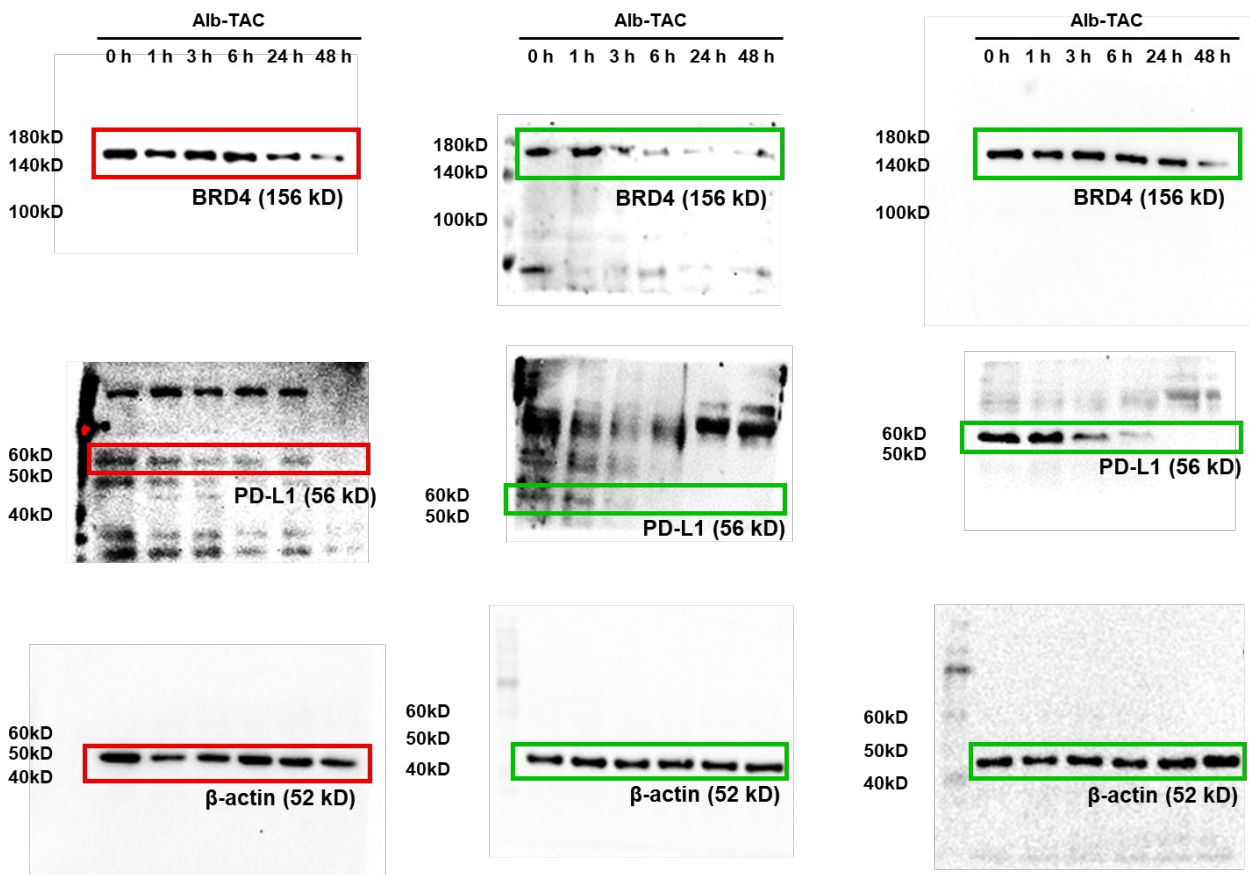


**Figure S35. Uncropped western blot results of Alb-TAC-treated samples in Figure S17B.**

Western blot analysis of 4T1 cells treated with 10  $\mu$ M Alb-TAC for different incubation times (0, 1, 3, 6, 24, and 48 h) to evaluate BRD4, PD-L1, and  $\beta$ -actin protein levels. Red boxes indicate the cropped regions presented in **Figure S17B**. Green boxes indicate the remaining two independent biological replicates. All data represent three independent biological replicates.

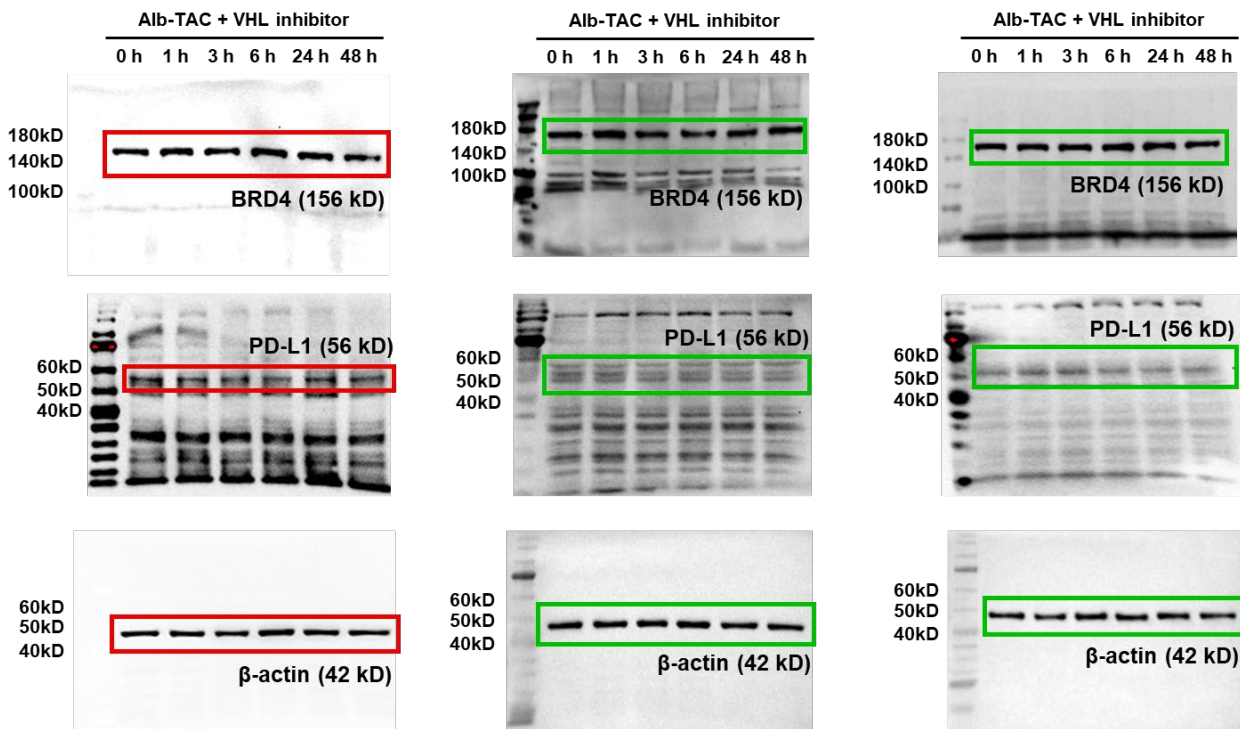


**Figure S36. Uncropped western blot results of Figure 3D.** Western blot analysis of CT26 cells treated with 10  $\mu\text{M}$  Alb-TAC with 50  $\mu\text{M}$  VHL inhibitor for different incubation times (0, 1, 3, 6, 24, and 48 h) to evaluate BRD4, PD-L1, and  $\beta$ -actin protein levels. Red boxes indicate the cropped regions presented in **Figure 3D**. Green boxes indicate the remaining two independent biological replicates. All data represent three independent biological replicates.

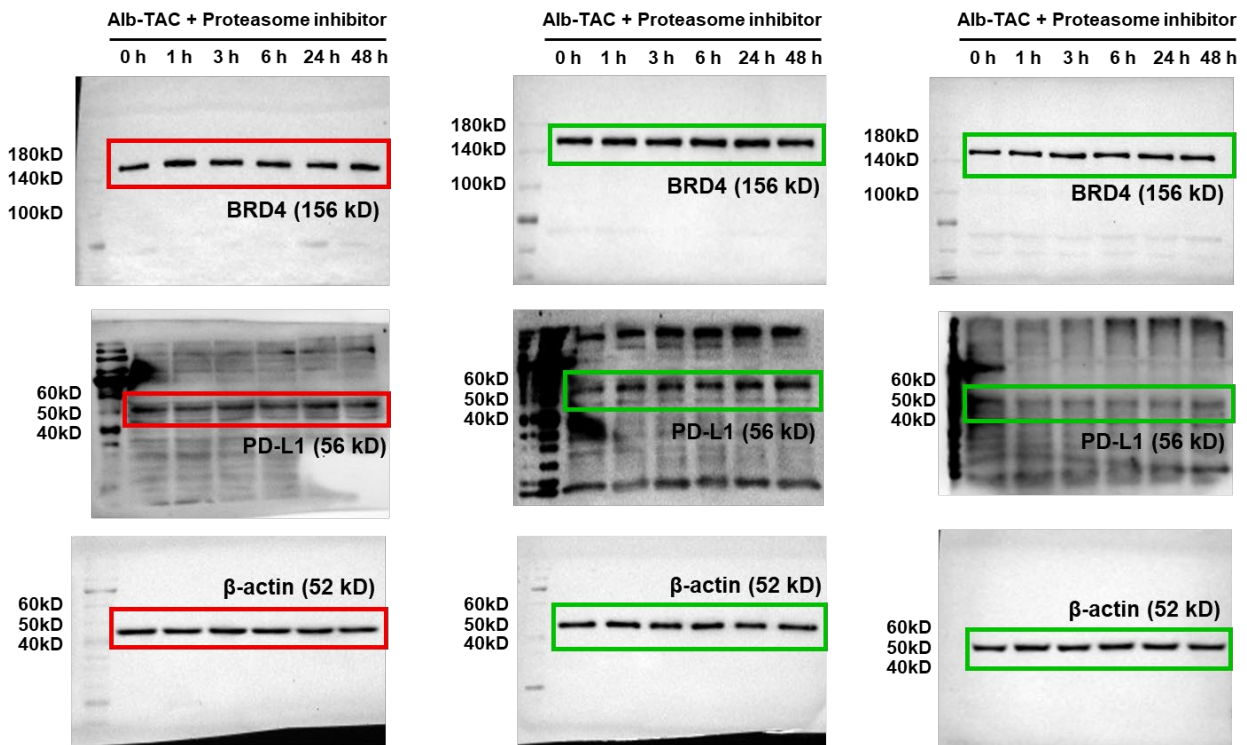


**Figure S37. Uncropped western blot results of Figure S19A.** Western blot analysis of CT26 cells treated with 10  $\mu$ M Alb-TAC with 10 nM proteasome inhibitor for different incubation times (0, 1, 3, 6, 24, and 48 h) to evaluate BRD4, PD-L1, and  $\beta$ -actin protein levels. Red boxes indicate the cropped regions presented in **Figure S19A**. Green boxes indicate the remaining two independent biological replicates. All data represent three independent biological replicates.

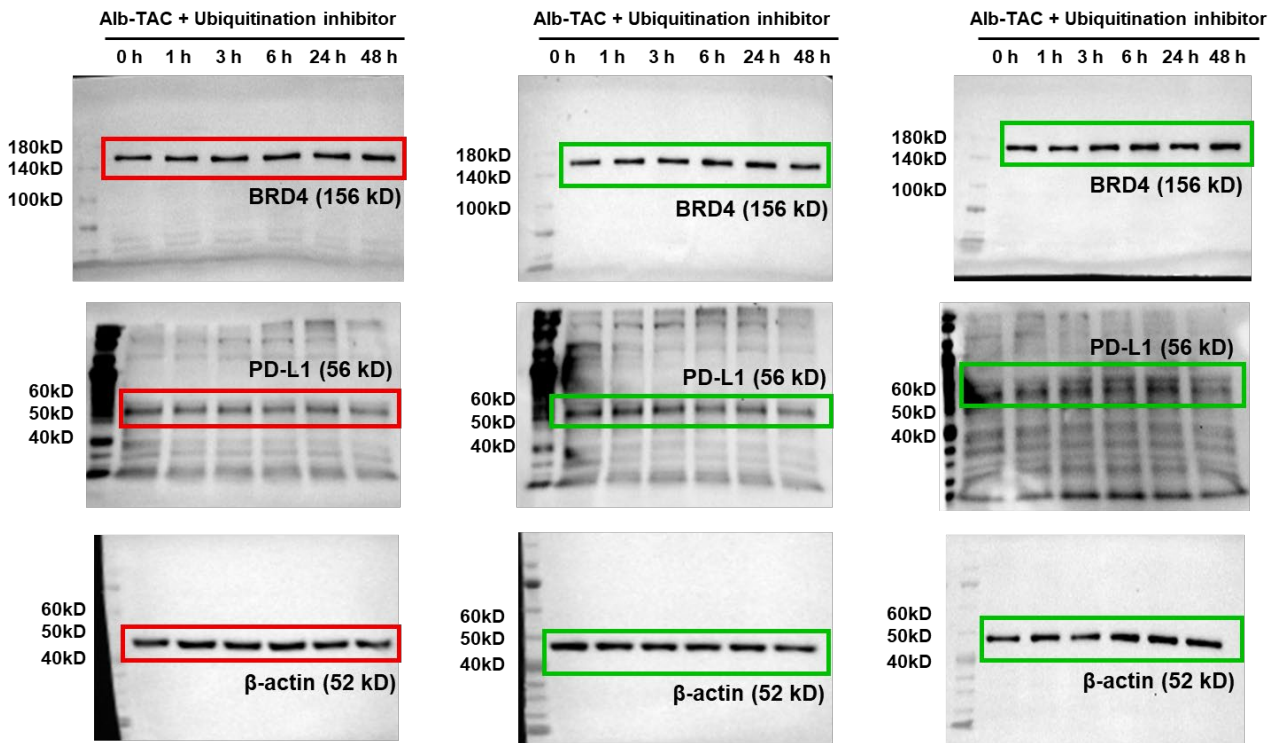


**Figure S38. Uncropped western blot results of Figure S19B.** Western blot analysis of CT26 cells treated with 10 μM Alb-TAC with 5 μM ubiquitination inhibitor for different incubation times (0, 1, 3, 6, 24, and 48 h) to evaluate BRD4, PD-L1, and β-actin protein levels. Red boxes indicate the cropped regions presented in **Figure S19B**. Green boxes indicate the remaining two independent biological replicates. All data represent three independent biological replicates.

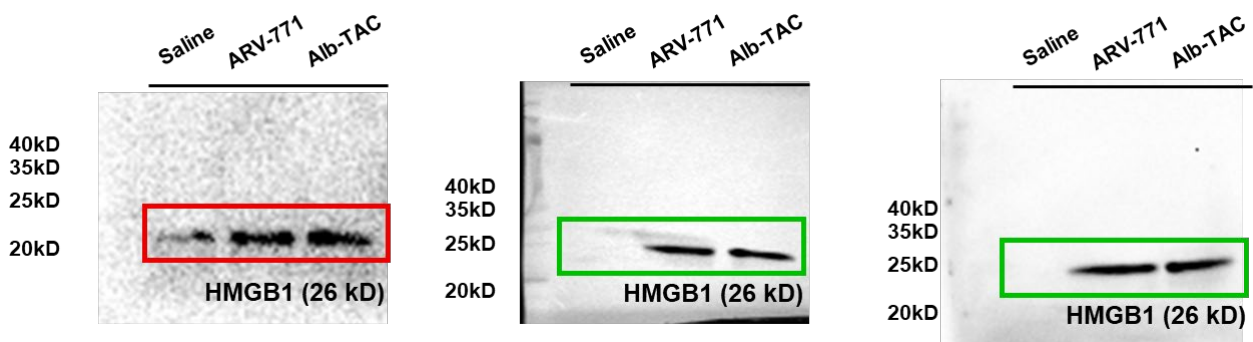


**Figure S39. Uncropped western blot results of Figure S20.** Western blot analysis of HMGB1 levels in culture supernatants collected from CT26 cells treated with saline, 10  $\mu$ M ARV-771, or 10  $\mu$ M Alb-TAC for 24 h. Red boxes indicate the cropped regions presented in **Figure S20**. Green boxes indicate the remaining two independent biological replicates. All data represent three independent biological replicates.

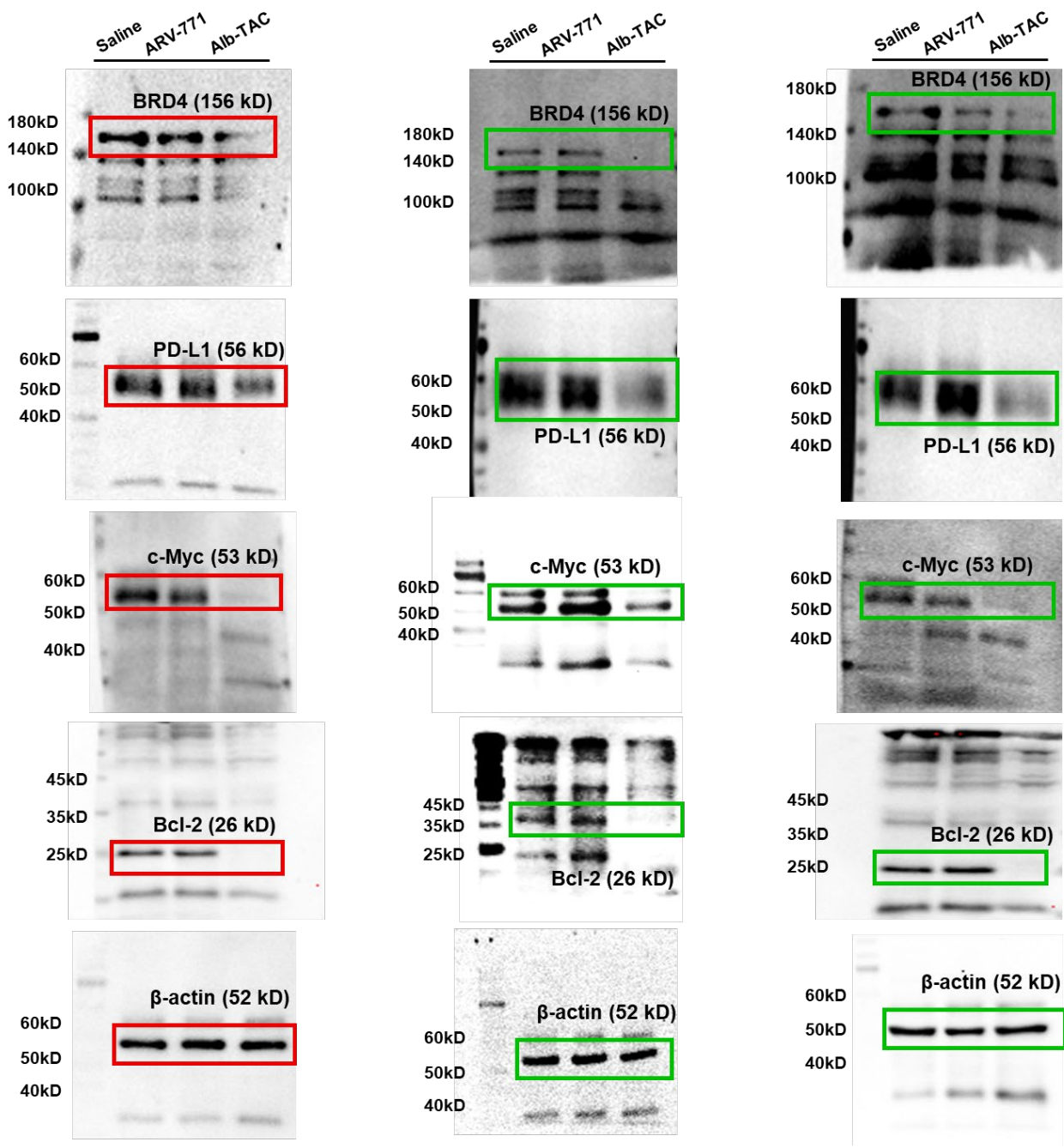


**Figure S40. Uncropped western blot results of Figure 5D.** Western blot analysis of tumor lysates from CT26 tumor-bearing mice in each group (saline, ARV-771 (10 mg/kg), and Alb-TAC (10 mg/kg)) showing expression of BRD4, PD-L1, c-Myc, Bcl-2, and  $\beta$ -actin protein levels. Red boxes indicate the cropped regions presented in **Figure 5D**. Green boxes indicate the remaining two independent biological replicates. All data represent three independent biological replicates.

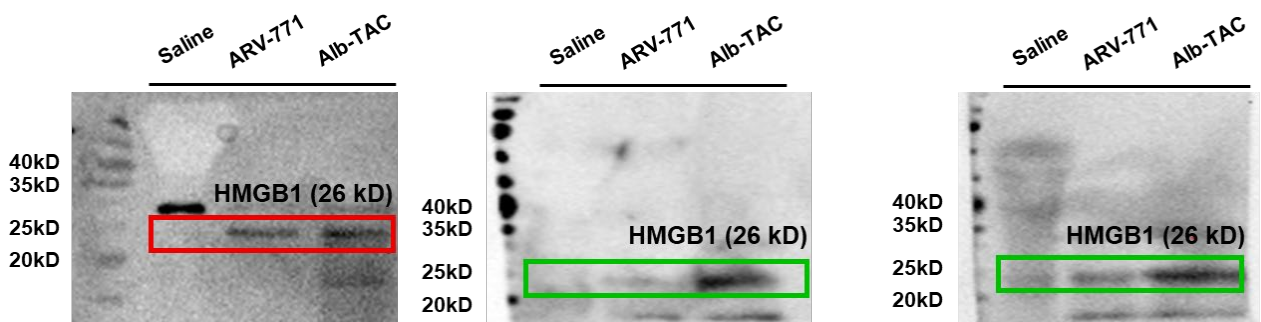


**Figure S41. Uncropped western blot results of Figure S23.** Western blot analysis of HMGB1 levels in tumor lysates from CT26 tumor-bearing mice in each group (saline, ARV-771 (10 mg/kg), and Alb-TAC (10 mg/kg)). Red boxes indicate the cropped regions presented in **Figure S23**. Green boxes indicate the remaining two independent biological replicates. All data represent three independent biological replicates.